

A Study of the Day - Night Effect for the Super - Kamiokande Detector: I. Time Averaged Solar Neutrino Survival Probability

Q.Y. Liu ^{a)}, M. Maris ^{a,b)}, S.T. Petcov ^{1 a,c)}

a) Scuola Internazionale Superiore di Studi Avanzati, Trieste, Italy.

b) INFN - Sezione di Pavia, Pavia, Italy.

c) INFN - Sezione di Trieste, Trieste, Italy.

Abstract

This is the first of two articles aimed at providing comprehensive predictions for the day-night (D-N) effect for the Super-Kamiokande detector in the case of the MSW $\nu_e \rightarrow \nu_{\mu(\tau)}$ transition solution of the solar neutrino problem. The one-year averaged probability of survival of the solar ν_e crossing the Earth mantle, the core, the inner 2/3 of the core, and the (core + mantle) is calculated with high precision (better than 1%) using the elliptical orbit approximation (EOA) to describe the Earth motion around the Sun. Results for the survival probability in the indicated cases are obtained for a large set of values of the MSW transition parameters Δm^2 and $\sin^2 2\theta_V$ from the “conservative” regions of the MSW solution, derived by taking into account possible relatively large uncertainties in the values of the ^8B and ^7Be neutrino fluxes. Our results show that the one-year averaged D-N asymmetry in the ν_e survival probability for neutrinos crossing the Earth core can be, in the case of $\sin^2 2\theta_V \leq 0.13$, larger than the asymmetry in the probability for (only mantle crossing + core crossing) neutrinos by a factor of up to six. The enhancement is larger in the case of neutrinos crossing the inner 2/3 of the core. This indicates that the Super-Kamiokande experiment might be able to test the $\sin^2 2\theta_V \leq 0.01$ region of the MSW solution of the solar neutrino problem by performing selective D-N asymmetry measurements.

¹ Also at: Institute of Nuclear Research and Nuclear Energy, Bulgarian Academy of Sciences, 1784 Sofia, Bulgaria.

1 Introduction

The Earth effect in neutrino propagation is a direct consequence of neutrino oscillations in matter [1]. If the neutrino mass spectrum is not degenerate and if neutrino mixing takes place in vacuum, the neutrino propagation is sensitive to the matter distribution along the propagation path and the probability to detect at Earth a ν_e produced in the Sun is a function of the detection time because at night the Sun is below the horizon and the solar neutrinos cross the Earth reaching the detector.

The observation of the Earth, or day-night (D-N), effect would be a proof of the validity of the MSW solution of the solar neutrino problem. In its simplest version the MSW mechanism involves matter - enhanced two-neutrino transitions of the solar ν_e into an active neutrino ν_μ or ν_τ , $\nu_e \rightarrow \nu_{\mu(\tau)}$, while the ν_e propagates from the central part to the surface of the Sun. The $\nu_e \rightarrow \nu_{\mu(\tau)}$ transition probability depends in this case on two parameters: Δm^2 and $\sin^2 2\theta_V$, where $\Delta m^2 > 0$ is neutrino mass squared difference and θ_v is the angle characterizing the neutrino mixing in vacuum. When the $\nu_{\mu(\tau)}$ produced in the Sun due to the MSW transitions and the solar ν_e not converted into $\nu_{\mu(\tau)}$ in the Sun cross the Earth, further $\nu_e \rightarrow \nu_{\mu(\tau)}$ transitions and/or ν_e regeneration due to the inverse MSW process $\nu_{\mu(\tau)} \rightarrow \nu_e$ can take place. This can lead to a difference between the signals caused by the solar neutrinos in a solar neutrino detector during the day and during the night, i.e., to a D-N asymmetry in the signal. No other mechanism of depletion of the solar ν_e flux proposed so far can produce such an effect.

The MSW solution of the solar neutrino problem and the D-N effect related to it have been extensively studied. The latest solar neutrino data can be described for values of the parameters Δm^2 and $\sin^2 2\theta_V$ belonging to the intervals [2]

$$\begin{aligned} 3.6 \times 10^{-6} \text{ eV}^2 \lesssim \Delta m^2 \lesssim 9.8 \times 10^{-6} \text{ eV}^2, \\ 4.5 \times 10^{-3} \lesssim \sin^2 2\theta_V \lesssim 1.3 \times 10^{-2}, \end{aligned} \tag{1}$$

or

$$\begin{aligned} 5.7 \times 10^{-6} \text{ eV}^2 \lesssim \Delta m^2 \lesssim 9.5 \times 10^{-5} \text{ eV}^2, \\ 0.51 \lesssim \sin^2 2\theta_V \lesssim 0.92, \end{aligned} \tag{2}$$

assuming the solar ν_e MSW transitions are into active neutrinos. The intervals (1) and (2) correspond to the nonadiabatic (small mixing angle) and to the adiabatic (large mixing angle) solutions of the solar neutrino problem. They have been obtained using the predictions of the solar model of Bahcall and Pinsonneault from 1995 [3] for the fluxes of the different solar neutrino flux components: pp, pep, ${}^7\text{Be}$, ${}^8\text{B}$ and CNO. This model takes into account heavy elements diffusion and was recently shown to be in very good agreement with the latest and more precise helio-seismological observations [4].

The possible solution values of Δm^2 and $\sin^2 2\theta_V$ are important in the calculations of the D-N effect because they determine the magnitude of the effect. A more conservative approach to the determination of the MSW solution regions of values of Δm^2 and $\sin^2 2\theta_V$

allows for, e.g., the spread in the predictions for the ^8B , ^7Be , etc. fluxes in the contemporary solar models, the possible changes in the predictions associated with the uncertainties in the relevant nuclear reaction cross-sections which are used as input in the flux calculations, etc.². Such an approach [5] yields larger regions for both the nonadiabatic and the adiabatic MSW solutions [2]:

$$\begin{aligned} 3.0 \times 10^{-6} \text{ eV}^2 \lesssim \Delta m^2 \lesssim 1.2 \times 10^{-5} \text{ eV}^2, \\ 6.6 \times 10^{-4} \lesssim \sin^2 2\theta_V \lesssim 1.5 \times 10^{-2}, \end{aligned} \tag{3}$$

or

$$\begin{aligned} 7.0 \times 10^{-6} \text{ eV}^2 \lesssim \Delta m^2 \lesssim 1.6 \times 10^{-4} \text{ eV}^2, \\ 0.30 \lesssim \sin^2 2\theta_V \lesssim 0.94. \end{aligned} \tag{4}$$

It is hardly conceivable at present that the values of Δm^2 and $\sin^2 2\theta_V$ for which the MSW $\nu_e \rightarrow \nu_{\mu(\tau)}$ transition mechanism provides a solution of the solar neutrino problem can be very different from those shown in Fig. 1 and given in equations (3) and (4).

The D-N effect was widely studied [6, 7, 8, 9, 10, 11, 12, 13, 14, 15]. It was pointed out, in particular, that the effect can be significant for $\sin^2 2\theta_V > 0.01$ for a large range of values Δm^2 and $\sin^2 2\theta_V$ from the large mixing angle solution region, for which the Earth effect regenerates electron neutrinos increasing the event rate at night. At the same time results from Kamiokande II and III experiments [16] did not reveal any significant Earth effect exceeding approximately 30%, thus excluding a rather large area of the region of values of Δm^2 and $\sin^2 2\theta_V$ of the large mixing angle solution [13]. This area is already excluded by the existing mean event rate data from the Cl-Ar, Ga-Ge and Kamiokande experiments.

The motivation for new quantitative theoretical studies of the D-N asymmetry comes from a number of considerations regarding the earlier studies and the experimental situation which is reasonable to expect in the near future. First of all the discovery of a D-N effect, even of a small one, should be an important confirmation of the neutrino oscillation hypothesis and will open a new chapter of physics, while the absence of any detectable effect should represent a strong constraint on the neutrino mass and mixing parameters relevant to the MSW solution. It is clear that in both cases quantitative predictions are required to assure a proper interpretation of experimental results. Second, most of the previous studies were primarily concerned with the nature of the effect [6, 8, 9, 10]. The relevant probability distributions and event rates were calculated for some representatives values of the parameters only, which is insufficient for a comprehensive understanding of the possible magnitude of the effect. Alternatively, in some of the articles on the subject the effect of the Earth on the oscillations of neutrinos was investigated for high energy neutrinos produced by cosmic rays or accelerators and the results obtained were extended to solar neutrinos [8, 17, 11, 18] (see also, e.g., [19]). The possible application of the Earth effect to the problem of the reconstruction of the Earth internal structure (Earth Tomography) was

²Although the total fluxes of ^8B , ^7Be , etc. neutrinos depend on the physical conditions in the central part of the Sun, the spectra of the ^8B , CNO and the pp neutrinos are solar physics independent.

also considered [17, 21, 22] (see also [8, 9, 11]). More detailed results on the Earth effect have been obtained in [12] where the D-N asymmetry for the Super - Kamiokande detector, for instance, was calculated for 8 (4) sets of values of $\sin^2 2\theta_V$ and Δm^2 from the region (1) ((2)) of the nonadiabatic (adiabatic) solution, as well as in [14] where the one year average iso - (D-N) asymmetry contours in the $\Delta m^2 - \sin^2 2\theta_V$ plane for the Super - Kamiokande and SNO detectors have been derived. Third, the Kamiokande experiment, like the other solar neutrino experiments which have provided data so far, has a relatively low statistics. This problem will be overcome by new experiments such as Super - Kamiokande, SNO and ICARUS. They are expected to be much more sensitive to the D-N effect, allowing to exploit a wider neutrino parameter region where the Earth effect is not large, in particular, the region of the small mixing angle nonadiabatic solution. One of them, Super - Kamiokande, is already operating and is expected to produce soon new results. Finally, an improved statistics allows to develop more sophisticated tests enhancing the sensitivity to the effect.

The present article represents the first of two articles aimed at providing comprehensive predictions for the D-N effect for the Super - Kamiokande detector in the case of the MSW $\nu_e \rightarrow \nu_{\mu(\tau)}$ transition solutions of the solar neutrino problem. These include: i) calculation of the Earth effect with a sufficiently high precision which can match the precision of the data on the effect to be provided by the Super - Kamiokande detector, ii) calculation of the magnitude of the effect for a sufficiently large and representative set of values of the parameters from the “conservative” regions (3) and (4) of the MSW solution, iii) calculations of the one-year averaged D-N asymmetry for solar neutrinos crossing the Earth mantle, the core, the inner 2/3 of the core, and the mantle + core (full Earth) for the chosen large set of values of Δm^2 and $\sin^2 2\theta_V$ with the purpose of illustrating the magnitude of the enhancement of the effect which can be achieved by an appropriate selection of the data sample, iv) calculation of the one year average deformations of the e^- spectrum by the Earth effect in the mantle, core, and in mantle + core for the selected representative set of values of Δm^2 and $\sin^2 2\theta_V$.

The magnitude of the D-N effect is determined by the MSW probability of solar ν_e survival when the solar neutrinos cross the Earth to reach the detector, $P_{\oplus}(\nu_e \rightarrow \nu_e)$, as well as by the probability of solar ν_e survival in the Sun, $\bar{P}_{\odot}(\nu_e \rightarrow \nu_e)$, describing the MSW effect on the solar neutrino flux detected during the day. Thus, the first step in the realization of our program of studies of the D-N effect consists of sufficiently precise calculation of the one year average probability $\bar{P}_{\oplus}(\nu_e \rightarrow \nu_e)$ in the cases of interest, i.e., for neutrinos crossing the mantle, the core, 2/3 of the core and the mantle + core when traversing the Earth. In the present article this first step is accomplished.

2 Calculating the Earth Effect

Given that Super - Kamiokande detector should have an event rate of about 10^4 solar neutrino induced events per year (with a 5 MeV energy threshold), the expected statistical accuracy in the flux measurement is about 1%. This means that the numerical accuracy in computing the Earth effect has to be better than approximately 1% each time the effect is not smaller than 1%.

Comprehensive and sufficiently accurate predictions require complex computations. In order to obtain detailed predictions for the magnitude of the D-N effect and how it changes with the change of the values of the two parameters Δm^2 and $\sin^2 2\theta_V$, we have chosen to

calculate the effect for a large set of points from the MSW solution regions (3) and (4). The values of Δm^2 and $\sin^2 2\theta_V$ corresponding to these points are given in Table I. The points selected are distributed evenly in the “conservative” regions of the nonadiabatic and the adiabatic solutions (3) and (4) [2].

We have used the Stacey model [23] as a reference model for the Earth density distribution in our calculations. Obviously, this is not an unquestionable choice because new models were produced in the last years (see, e.g., [24]). However, the merit of the Stacey model when compared with alternative ones is its ability to describe the known details of the Earth radial density distribution, $\rho(R)$, relevant for the Earth effect calculations. This is done through a set of polynomials which allows the use of very efficient numerical computation schemes. In the Stacey model the Earth is assumed to be spherical and isotropical with a radius of 6371 km. As in all Earth models, there are two main density structures in the Stacey model: mantle and core. The core has a radius of 3485.7 km and a mean density of approximately 11.5 gr/cm³. The mantle surrounding the core has a mean density of about 4 gr/cm³. Both of them have a number of density substructures.

The Earth effect formalism was described by many authors and it was reviewed recently in ref. [12]. The probability that an electron neutrino produced in the Sun will not be converted into $\nu_{\mu(\tau)}$ when it propagates in the Sun and traverses the Earth on the way to the detector is given by [7]

$$P_{\oplus}(\nu_e \rightarrow \nu_e) = \bar{P}_{\odot}(\nu_e \rightarrow \nu_e) + \frac{1 - 2\bar{P}_{\odot}(\nu_e \rightarrow \nu_e)}{\cos 2\theta_V} (P_{e2} - \sin^2 \theta_V), \quad (5)$$

where $\bar{P}_{\odot}(\nu_e \rightarrow \nu_e)$ is the average probability of solar ν_e survival in the Sun and P_{e2} is the probability of the $\nu_2 \rightarrow \nu_e$ transition after the ν_e have left the Sun. During the day, when the neutrinos do not cross the Earth, $P_{e2} = \sin^2 \theta_V$ and we have $P_{\oplus}(\nu_e \rightarrow \nu_e) = \bar{P}_{\odot}(\nu_e \rightarrow \nu_e)$. For Earth crossing neutrinos at night $P_{e2} \neq \sin^2 \theta_V$ due to the MSW effect and $P_{\oplus}(\nu_e \rightarrow \nu_e) \neq \bar{P}_{\odot}(\nu_e \rightarrow \nu_e)$. Throughout this study we use for $\bar{P}_{\odot}(\nu_e \rightarrow \nu_e)$ the expression derived in ref. [25] in the exponential approximation for the variation of the electron number density, N_e , along the neutrino path in the Sun:

$$\bar{P}_{\odot}(\nu_e \rightarrow \nu_e) = \frac{1}{2} + \left(\frac{1}{2} - P' \right) \cos 2\theta_V \cos 2\theta_m, \quad (6)$$

where θ_m is the neutrino mixing angle in matter at the point of ν_e production in the Sun and

$$P' = \frac{e^{-2\pi r_0 \frac{\Delta m^2}{2E}} \sin^2 2\theta_v - e^{-2\pi r_0 \frac{\Delta m^2}{2E}}}{1 - e^{-2\pi r_0 \frac{\Delta m^2}{2E}}} \quad (7)$$

is the analog of the Landau-Zener jump probability for exponentially varying N_e , r_0 being the scale height characterizing the change of N_e along the neutrino trajectory. The probability $\bar{P}_{\odot}(\nu_e \rightarrow \nu_e)$, eq. (6), was averaged over the region of ⁸B neutrino production in the Sun. For values of $\sin^2 2\theta_V \lesssim 4 \times 10^{-3}$ the probability $\bar{P}_{\odot}(\nu_e \rightarrow \nu_e)$ was calculated following the prescriptions given in [26].

Let us discuss next the calculation of the probability P_{e2} . In contrast to $\bar{P}_{\odot}(\nu_e \rightarrow \nu_e)$, the probability P_{e2} is not a constant in time because it is a function of the trajectory followed by the neutrinos crossing the Earth. The latter is determined by the instantaneous apparent position of the Sun in the sky. Given the fact that data are taken over a certain interval of time, the instantaneous P_{e2} in eq. (5) has to be replaced with its time averaged, $\langle P_{e2} \rangle$, which requires the computation of the apparent solar trajectory in the detector sky.

The exact solar trajectory is a complicated function of time which changes with the epoch of the year and the geographical location. Its computation is described in Appendix A, while for the present discussion it is enough to recall its main features.

Looking at the Sun as at a star projected on a sphere centered on the detector location, its position is specified by a couple of spherical co-ordinates [27, 36]. Assuming the Earth is a spherical and isotropical body, the Sun's Nadir angle is enough to describe the Sun position in order to compute the probability P_{e2} . The *Nadir angle* \hat{h} is the angle subtended by Sun's and Earth center directions as seen from the detector ³, as depicted in Fig. 1. During the day \hat{h} is greater than 90° (and $P_{e2} \equiv \sin^2 \theta_V$), while at night $\hat{h} \leq 90^\circ$, the Sun rises or sets when $\hat{h} = 90^\circ$ and a solar neutrino will cross the Earth center when $\hat{h} = 0^\circ$.

The Sun's apparent trajectory in the sky with respect to the detector is a function of the day of the year d . Each night the Sun reaches a minimum Nadir angle, $\hat{h}_{m,d}$. In the course of the year $\hat{h}_{m,d}$ has a maximum value, $\hat{h}_{m,max}$, and a minimum value, $\hat{h}_{m,min}$. Thus, given a point in the interior of the Earth seen (with respect to the detector) along a line of view of Nadir angle \hat{h} , it will never be on the solar neutrino trajectory during the night if $\hat{h} < \hat{h}_{m,min}$; it will be on a trajectory for some of the nights during the year if $\hat{h}_{m,min} \leq \hat{h} < \hat{h}_{m,max}$, while if $\hat{h} \geq \hat{h}_{m,max}$ it will be crossed by neutrinos every night.

These limits and the apparent trajectory of the Sun, are functions of the detector location specified by its latitude, λ_D , and longitude. For a detector outside the tropical band, $|\lambda_D| > 23^\circ 27'$, $\hat{h}_{m,max}$ is reached at summer solstice, $\hat{h}_{m,min}$ is reached at winter solstice, and $\hat{h}_{m,min} > 0^\circ$ so that neutrinos received by such detectors never cross the Earth center. Instead, for detectors located inside the tropical band, $\hat{h}_{m,min} = 0^\circ$ and neutrinos crossing the Earth center are detected, while the minimum and maximum night Nadir angle are reached at epochs between equinoxes and solstices. At last for an equatorial detector $\hat{h} = 0^\circ$ is reached just at equinoxes.

It is well know that for a real time detector as Super - Kamiokande it is possible to compute \hat{h} for the Sun at the time t of the detection of a given event, allowing the selection of events produced when the Sun is seen within a given Nadir angle interval $[\hat{h}_1, \hat{h}_2]$. The boundaries of this interval are crossed at times \hat{t}_1 and \hat{t}_2 . As will be shown further, this selection may be a feasible strategy to increase the sensitivity to the D-N effect.

It follows from the above discussion that in order to take into account the Earth effect in the signal collected in the time interval $[T_1, T_2]$ of the year by a given detector it is enough to replace P_{e2} in eq. (5) with its time averaged $\langle P_{e2} \rangle$ defined as:

$$\langle P_{e2} \rangle = \frac{1}{T_{res}} \int_{T_1}^{T_2} dt \delta(\hat{h}_1 \leq \hat{h}(t) \leq \hat{h}_2) P_{e2}(\hat{h}(t)), \quad (8)$$

³In a Local Reference Frame centered on the detector D (see Fig. 1) the *Nadir* is the point on the celestial sphere which lies below the detector along its vertical axis, i.e., it is the point opposite to the detector Zenith.

where $[\hat{h}_1, \hat{h}_2]$ is the Nadir angle interval of interest, $\hat{\delta}$ is the sampling function and

$$T_{res} = \int_{T_1}^{T_2} dt \hat{\delta}(\hat{h}_1 \leq \hat{h}(t) \leq \hat{h}_2) \quad (9)$$

is the *residence time*, i.e., the time spent by the Sun in the Nadir angle interval.

The values of $\langle P_{e2} \rangle$ and T_{res} are functions of the Nadir angle interval, the time interval and of the sampling scheme described by the sampling function. Here it is assumed that the sampling i) is continuous over the time interval in which the Sun is in the relevant Nadir angle interval $[\hat{h}_1, \hat{h}_2]$, ii) is extended over an integer set of years, and iii) that the error in the reconstruction of the apparent Sun position at the time of the detection of each solar neutrino event is negligible. With these hypotheses $\hat{\delta}(\hat{h}_1 \leq \hat{h} \leq \hat{h}_2)$ is 1 when \hat{h} is inside the interval $[\hat{h}_1, \hat{h}_2]$ and zero otherwise.

The choice of the Nadir angle interval is quite arbitrary, but a natural one is to compare data collected at *Day* ($\hat{h} > 90^\circ$) with data collected during the full *Night* ($0^\circ \leq \hat{h} \leq 90^\circ$), and to separate neutrinos detected at night into *Core* neutrinos, $0^\circ \leq \hat{h} \leq \hat{h}_c$, and *Mantle* neutrinos, $\hat{h}_c \leq \hat{h} \leq 90^\circ$, where $\hat{h}_c = 33.17^\circ$ is the apparent Nadir angle of the core/mantle boundary in the Stacey model. The three averages are labeled respectively: $\langle P_{e2} \rangle^C$, $\langle P_{e2} \rangle^M$ and $\langle P_{e2} \rangle^N$, while the corresponding residence times are labeled T_{res}^C , T_{res}^M ; the *Night* residence time T_{res}^N is identical to half an year for any detector. The day averaged probability $\langle P_{e2} \rangle_{day}$ coincides with $\sin^2 \theta_V$. Finally, it is possible to consider also the *Deep - Core* average probability for which the Nadir angle interval in eq. (8) is $\hat{h}_{m,min} \leq \hat{h} \leq 2/3\hat{h}_c$. The symbols *Day*, *Night*, *Mantle*, *Core* and *Deep - Core* will be used in what follows to indicate these particular solar neutrino event samples.

In the absence of neutrino oscillations the number of solar neutrinos induced events in a given Nadir angle interval is proportional to T_{res} for that interval. Table II lists a set of residence times for the Super - Kamiokande detector, showing that in one year, for approximately 14% of the total night time the Sun is seen behind the Earth core, so that about 7% of neutrinos cross the core. With a statistics of 10^4 events this corresponds to a relative statistical error of about 3.8%.

The residence time is also relevant because it determines the weight of the contribution of each geophysical structure s , $s = \text{Night, Mantle, Core, Deep - Core}$, to $\langle P_{e2} \rangle^N$, the contribution being proportional to the ratio $T_{Resid}^s/T_y/2$, where $T_y = 365.24$ days. Thus, for the Super - Kamiokande detector the *Core* contribution in $\langle P_{e2} \rangle^N$ has to be weighted by the factor 0.07 and it is no longer a dominant contribution even when $\langle P_{e2} \rangle^C$ is much larger than $\langle P_{e2} \rangle^M$.

Many types of systematic errors can affect the predictions for the D-N asymmetry. Among them the detector specifications such as detection efficiency, energy resolution, etc. are undoubtedly very important. They are neglected in the present study because they are not yet exactly known for the Super - Kamiokande detector, and moreover they may change during the various phases of data taking. In this case the only experimental feature to be taken into account is the energy threshold, while the most relevant error sources which have to be discussed are the numerical errors and the Sun's apparent motion reconstruction. Let us add that the error introduced by uncertainties in the detection cross section for the $\nu_e - e^-$ elastic scattering process is less than 1% [28] and is neglected. The same is true also for the detector location which is known with an accuracy better than 1 arcmin or 1 over 10^4 [29].

The choice of a correct approximation for the apparent solar motion is a crucial point in order to reach the required accuracy, given the Earth model used in the calculations. The motion is quite complex and approximations are required to obtain an acceptable computation time but at the price of a certain error. There are two kinds of approximation made which are relevant for the Earth effect. In the first the Earth motion around the Sun is circular (COA), in the second elliptical (EOA). Neither the first nor the second are exact models, but EOA is very accurate for Earth effect prediction purposes. The analysis (see Appendix 6) shows that most of the errors introduced by COA and EOA are periodic in nature, so that in the turn of one year they should be averaged out. However, given that P_{e2} is a function of the solar position and that the use of different sampling schemes (as *Core*, *Mantle*, *Night*, etc.) are equivalent to averaging over specific fractions of the time of the year only, it is not possible to test such approximations without accurate numerical experiments. These experiments show that indeed the error introduced by the simpler COA model can be close to (but does not exceed) 1%, and that a greater accuracy is reached by EOA. In this way the use of EOA for all the computations presented in this paper and in [30] assures an accuracy better than 1% for each kind of sampling. The COA can be used when a large amount of simulations are required, allowing a substantial reduction of the computational time but at the cost of an increase in the error in $\langle P_{e2} \rangle$, which can reach 0.8%.

In the Elliptical Orbit Approximation the averaged probabilities and residence times defined by (8) have to be modified to take into account the change in the Sun - Earth distance with time, which causes a periodical change in the solar neutrino flux and in the Earth orbital velocity. To take both effects into account it is not enough to replace the relation between \hat{h} and the time of the year t , but also the form of (8) has to be adapted. Let $R(t)$ be the time dependent Sun - Earth distance expressed in units of the mean distance (the Astronomical Unit $R_0 = 1.4966 \times 10^8$ km). Then each instantaneous sample has to be weighted by the factor $1/R^2(t)$ leading to:

$$\begin{aligned} \langle P_{e2} \rangle &= \frac{1}{T_{res}} \int_{T_1}^{T_2} dt \frac{\delta(\hat{h}_1 \leq \hat{h}(t) \leq \hat{h}_2)}{R^2(t)} P_{e2}(\hat{h}(t)), \\ T_{res} &= \int_{T_1}^{T_2} dt \frac{\delta(\hat{h}_1 \leq \hat{h}(t) \leq \hat{h}_2)}{R^2(t)}. \end{aligned} \tag{10}$$

As it is discussed in Appendix 6, the effect of the factor $1/R^2$ is partially compensated by the change in the residence time due to the change of the Earth orbital velocity during the year.

3 The Instantaneous P_{e2} Probability

At the basis of each time averaged probability $\langle P_{e2} \rangle$ is the instantaneous one, P_{e2} . Many features of $\langle P_{e2} \rangle$ are a direct consequence of those present in P_{e2} . It is natural to begin the discussion of our numerical results with those obtained for P_{e2} .

Figure 2 shows an example of the probability P_{e2} for $\sin^2 2\theta_V = 0.01$ as a function of the *resonance density* ρ_R which is connected to E and the neutrino transition parameters Δm^2 and $\sin^2 2\theta_V$ through the resonance condition:

$$\rho_R Y_e = 6.57 \times 10^6 (\Delta m^2 / E_\nu) \cos 2\theta_V, \quad (11)$$

where ρ_R is expressed in gr/cm^3 , E_ν in MeV, Δm^2 in eV^2 , Y_e is the electron fraction per nucleon. We have for the Earth $Y_e = 1/2$ with a rather high accuracy. For a fixed $\cos 2\theta_V$ equation (11) justifies the use of ρ_R as an independent variable instead of $E/\Delta m^2$. The probability P_{e2} as a function of ρ_R was computed solving the two-neutrino propagation equation [31, 32] using a 4th order, adaptive step-size Runge - Kutta algorithm adapted from [33]. Each plot in Fig. 2 refers to a different Nadir angle. There are two main peaks, \mathcal{C} (at $\rho_R \cong (10 - 11) \text{ gr}/\text{cm}^3$) and \mathcal{M} (at $\rho_R \cong (4 - 6) \text{ gr}/\text{cm}^3$), associated with resonant transitions in the core (\mathcal{C}) and in the mantle (\mathcal{M}). This correspondence is based on the following observations: i) a geological structures is relevant for the neutrino transitions (and therefore for P_{e2}) when neutrinos cross it, ii) the structure affects the neutrino propagation when its density is the resonance region for the crossing neutrinos, iii) when one of the previous conditions are not fulfilled P_{e2} is close to its vacuum value $\sin^2 \theta_V$. When $\sin^2 2\theta_V$ increases, for instance, the resonance width also increases and it is possible to have a rather large P_{e2} for values of ρ_R which do not correspond to any density crossed by neutrinos along their trajectory. In addition, the spherical symmetry of the Earth implies that solar neutrinos will cross the resonance region twice. This can produce interference terms in P_{e2} leading to oscillatory dependence of P_{e2} on \hat{h} for a fixed ρ_R [12]. They can also be responsible for the presence of multiple peaks in P_{e2} as a function of ρ_R for a fixed \hat{h} , associated with the resonances in a given geological structure. An example of this possibility is the splitting of the core peak \mathcal{C} in Fig. 2(a) in two peaks, C_I and C_O , shown in Fig. 2(c). Indeed, it is reasonable to expect the interference terms in P_{e2} to be significant in certain cases because the neutrino oscillation length in matter for solar neutrinos which undergo resonant transitions in the Earth is of the order of the Earth radius.

It is instructive to see how the P_{e2} dependence on ρ_R changes with the increasing of $\sin^2 2\theta_V$. For $\sin^2 2\theta_V < 0.1$ the qualitative properties of this dependences do not change significantly: P_{e2} is basically “rescaled” in accordance with the change of $\sin^2 2\theta_V$ and $(P_{e2} - \sin^2 \theta_V)$ goes to zero rather quickly outside the resonance region. For larger values of $\sin^2 2\theta_V$ the behavior is more complicate because new peaks appear, becoming more and more prominent as $\sin^2 2\theta_V$ increases. The “scaling” of P_{e2} is not precise, different parts of the plot scale differently, as is well illustrated by the \mathcal{C} and \mathcal{M} peak heights. With the rise of $\sin^2 2\theta_V$ \mathcal{C} increases faster than \mathcal{M} reaching a maximum value and begins to decrease while \mathcal{M} is still increasing. As a consequence, at values of $\sin^2 2\theta_V \lesssim 0.13$ most of the D-N asymmetry is generated by the MSW effect in the core. This is not true in the large mixing angle region. For practical purposes the most important lesson which can be drawn from the P_{e2} plots is that to produce accurate predictions for the Earth effect, P_{e2} has to be computed for resonance densities ρ_R (or equivalently, for values of $E/\Delta m^2$) which are largely outside the density range of the Earth geological structures.

4 Averaging the P_{e2} Probability

Figures 3.1 - 3.18 depict the results of numerical calculations of $\langle P_{e2} \rangle$ and P_\oplus for the Super - Kamiokande detector in the case of solar ν_e transitions into an active neutrino ⁴,

⁴See appendix 6 for further details.

$\nu_e \rightarrow \nu_{\mu(\tau)}$. Each figure is divided into four “frames” which are labeled (a), (b), (c) and (d). Figures 3.1a - 3.18a display $\langle P_{e2} \rangle$ for *Night* (short-dashed line), *Mantle* (dotted line), *Core* (solid line) and *Deep - Core* (long-dashed line) as a function of ρ_R and are the subject of the discussion in this Section. Comparing $\langle P_{e2} \rangle$ with P_{e2} shown in Fig. 2, it is possible to identify the peak due to the resonance in the mantle, M , present also in P_{e2} . Similarly, there are two very well defined peaks (or a peak, C , with two maxima) in $\langle P_{e2} \rangle$, C_I (at larger ρ_R) and C_O (at smaller ρ_R), which correspond to the resonance in the core.

The presence of wiggles is evident for ρ_R greater than the core density, especially at large mixing angles. These wiggles are damped and disappear as ρ_R increases. A curious feature is that in most of the cases the wiggles come in triplets (see Fig. 3.14a). The Log-Log plots of the $\langle P_{e2} \rangle$ probability (not reported here) show that for ρ_R outside the range of the Earth density $\langle P_{e2} \rangle$ decreases as follows:

$$\log \left(\frac{\langle P_{e2} \rangle}{\sin^2 \theta_V} - 1 \right) = A + B \log \rho_R + \epsilon f(\rho_R), \quad (12)$$

where A , B and ϵ are real constants and $f(\rho_R)$ is a damped oscillating function which represents the wiggles. Since ϵ is small ($\lesssim 10^{-2}$), $f(\rho_R)$ can be neglected, while A and B can be determined by numerical means for any $\langle P_{e2} \rangle$. Equation (12) is used to extrapolate $\langle P_{e2} \rangle$ at values of ρ_R far from the Earth density.

As Figs.3.1a - 3.18a illustrate, the separation in *Core* and *Mantle* samples is very effective in enhancing $\langle P_{e2} \rangle$. The enhancement is particularly large for small mixing angles for which $\langle P_{e2} \rangle^C$ can be up to six times bigger than $\langle P_{e2} \rangle^M$. This suggests the possibility of a corresponding enhancement of the e^- -spectrum distortions as well as of the energy integrated event rate. The latter can make feasible the detection of the Earth effect even at small mixing angles. Further enhancement of the probability $\langle P_{e2} \rangle$ can take place if the size of the core bin is decreased, as shown by the *Deep - Core* averaged probability plotted with a long-dashed line. However, the reduction in the bin size reduces the residence time in the *Deep - Core* bin to less than 4% per year and it is not clear whether the probability enhancement can compensate the corresponding reduction in statistics.

5 The Solar ν_e Survival Probability

The connection between the peak structures in the probabilities $\langle P_{e2} \rangle$ and P_{\oplus} considered as functions of $E/\Delta m^2$, is determined basically by eq. (5). The presence of an enhancement in the averaged probability $\langle P_{e2} \rangle$ is not enough to ensure an enhancement in the D-N asymmetry. This is especially true at small mixing angles at which the Earth effect may produce reduction instead of increase of the ν_e flux. The latter happens when $\bar{P}_{\odot} > 0.5$, so that most of neutrinos coming from the Sun are ν_1 which are converted into ν_{μ} , ν_{τ} in the Earth.

The upper parts (“windows”) of the “frames” (b), (c) and (d) shown in Figs. 3.1 - 3.18 are combined plots of \bar{P}_{\odot} (dotted line), P_{e2} (dashed line) and P_{\oplus} (solid line) for *Night* (b), *Core* (c) and *Mantle* (d) as functions of $E/\Delta m^2$. The lower “windows” of each “frame” are plots of the ratio:

$$\mathcal{A}_P \equiv 2 \frac{P_{\oplus} - \bar{P}_{\odot}}{P_{\oplus} + \bar{P}_{\odot}} \quad , \quad (13)$$

which mimics the asymmetry used by the Kamiokande collaboration in their discussion of the D-N effect. This quantity will also be called *asymmetry*. In some cases $\langle P_{e2} \rangle$ is too small to be visible in the full scale plot, and so it is rescaled by a factor of 10. This is indicated by the label “ $\langle P_{e2} \rangle \times 10$ ” in the upper right corner of the corresponding figure.

The purpose of these figures is to illustrate how each probability contributes in P_{\oplus} and in the asymmetry \mathcal{A}_P . One of the important features that has to be taken into account in the discussion of P_{\oplus} is the position of the peaks in $\langle P_{e2} \rangle$ with respect to the value of $E/\Delta m^2$ at which $\bar{P}_{\odot} = 0.5$ because it controls the sign and the magnitude of the D-N effect. It follows from eq. (5) that the asymmetry is zero each time $\bar{P}_{\odot} = 0.5$ irrespective of the value of $\langle P_{e2} \rangle$. If $\langle P_{e2} \rangle > \sin^2 \theta_V$, but $\bar{P}_{\odot} > 0.5$, the asymmetry is negative which means the Earth effect *reduces* the night event rate instead of *increasing* it. The positive Earth effects occurs when $\bar{P}_{\odot} < 0.5$, i.e., when the peak of $\langle P_{e2} \rangle$ falls inside the lower part of the “pit” of the MSW probability \bar{P}_{\odot} . Figures 3.1 - 3.18 illustrate all these possibilities together with less relevant cases corresponding to $\langle P_{e2} \rangle = \sin^2 \theta_V$ and $\langle P_{e2} \rangle < \sin^2 \theta_V$. The presence of a zero Earth effect line together with cases in which the asymmetry \mathcal{A}_P as a function of $E/\Delta m^2$, can be both negative and positive, can reduce the magnitude of the Earth effect. This reduction is especially important at small mixing angles.

The increase of $\sin^2 2\theta_V$ within the small mixing angle solution region (3) does not change considerably the minimum and maximum values of \bar{P}_{\odot} , but it affects significantly the width of the “pit” of \bar{P}_{\odot} . At the same time the peaks in $\langle P_{e2} \rangle$ change mainly their height and width but not their position with respect to the $E/\Delta m^2$ axis. For $\sin^2 2\theta_V \leq 0.002$ most of the relevant part of $\langle P_{e2} \rangle$ is confined in the $\bar{P}_{\odot} > 0.5$ region and the Earth effect is negative. With the increase of $\sin^2 2\theta_V$ the \bar{P}_{\odot} “pit” becomes wider. Correspondingly, larger parts of the $\langle P_{e2} \rangle$ peak enter the $\bar{P}_{\odot} < 0.5$ region: depending on the value of $E/\Delta m^2$, the asymmetry \mathcal{A}_P (the Earth effect) can be negative or positive. This continues until $\sin^2 2\theta_V \cong 0.006$, for which most of the $\langle P_{e2} \rangle$ peak is in the $\bar{P}_{\odot} < 0.5$ region and the effect is mostly positive. This implies that even if $\langle P_{e2} \rangle$ is relatively large, there will be a region at small mixing angles where the asymmetry is zero and the *Core* enhancement is not effective.

The sequence of \mathcal{A}_P plots allows to identify various peak components which we will denote by \mathcal{A} , \mathcal{H}^+ , \mathcal{H}^- , \mathcal{A} being the left one (located at smaller values of $E/\Delta m^2$), while \mathcal{H}^+ (\mathcal{H}^-) is located at larger $E/\Delta m^2$ in the region where $\mathcal{A}_P > 0$ ($\mathcal{A}_P < 0$). The \mathcal{A} structure is an artifact of the presence of the adiabatic minimum in the probability \bar{P}_{\odot} , $\min \bar{P}_{\odot} = \sin^2 \theta_V$, which can lead to a relatively large asymmetry \mathcal{A}_P even if $\langle P_{e2} \rangle$ is small. The smallness of $\langle P_{e2} \rangle$ in the \mathcal{A} region means that that this region does not contribute significantly to the total event rate asymmetry.

The bulk of the D-N asymmetry comes from \mathcal{H}^- and \mathcal{H}^+ structures, which are directly connected to the C and M peaks in $\langle P_{e2} \rangle$. For $\sin^2 2\theta_V \leq 0.002$ (Figs. 3.1 - 3.3) most of the peaks in $\langle P_{e2} \rangle$ lie in the $\bar{P}_{\odot} > 0.5$ region. Correspondingly, the asymmetry \mathcal{A}_P is negative (only the peak \mathcal{H}^- is present). It increases in absolute value as $\sin^2 2\theta_V$ increases and it is sensitive to the *Core* enhancement. As $\sin^2 2\theta_V$ grows further, the bulk of the $\langle P_{e2} \rangle$ resonance part enters the region where $\bar{P}_{\odot} = 0.5$, producing a suppression of the

asymmetry and of the *Core* enhancement, as is illustrated for $\sin^2 2\theta_V = 0.004$ in Fig. 3.4. It is interesting to note that this crossing occurs at different $\sin^2 2\theta_V$ for the *Night*, *Core* and *Mantle* samples. As is shown in Fig. 3.4(c), the peak C for the *Core* is nearly cut in two parts by the $\bar{P}_\odot = 0.5$ line. This leads to the presence of both positive and negative Earth effect in the asymmetry \mathcal{A}_P , while in the cases of *Night* and *Mantle* (Figs. 3.4(b) and 3.4(d)) the asymmetry is negative. At $\sin^2 2\theta_V = 0.006$ (Fig. 3.5) the peak C is in the $\bar{P}_\odot < 0.5$ region while the bulk of the effect of the *Mantle* is still in the $\bar{P}_\odot \geq 0.5$ region. The *Core* asymmetry is positive and it has a maximum value of 16.4%. For $\sin^2 2\theta_V \geq 0.008$ (Figs. 3.6 - 3.18) the effect is positive. All these details are influenced by the position of the $\bar{P}_\odot = 0.5$ line with respect to the region of the $\langle P_{e2} \rangle$ maxima. Given the fact that the latter is primarily a function of the Earth model, it cannot be excluded that certain aspects of the behavior described above may change somewhat with the change of the Earth model used in the calculations.

Finally, the sequences of figures 3 show that the resonance in the core is the dominant source of the asymmetry in the region of the nonadiabatic solution, $\sin^2 2\theta_V \leq 0.013$ while for $\sin^2 2\theta_V \geq 0.3$ the bulk of the asymmetry is generated by the resonance in the mantle (the M peak) and the *Core* enhancement is only of the order of $30 \div 40\%$.

6 Conclusions

In the present article and in ref. [30] we have performed a detailed study of the D-N effect for the Super - Kamiokande detector assuming the MSW solution of the solar neutrino problem corresponding to solar ν_e transitions into an active neutrino, $\nu_e \rightarrow \nu_{\mu(\tau)}$. Among our aims were: i) calculation of the Earth effect with a sufficiently high precision which can match the precision of the data on the effect to be provided by the Super - Kamiokande detector, ii) calculation of the magnitude of the effect for a sufficiently large and representative set of values of the parameters from the “conservative” regions (3) and (4) of the MSW solution, iii) calculations of the one-year averaged D-N asymmetry for solar neutrinos crossing the Earth mantle, the core, the inner 2/3 of the core, and mantle + core (full Earth) for the chosen large set of values of Δm^2 and $\sin^2 2\theta_V$ with the purpose of illustrating the magnitude of the enhancement of the effect which can be achieved by an appropriate selection of the data sample, iv) calculation of the one-year average deformations of the e^- spectrum by the Earth effect in the mantle, the core, and in the mantle + core for the selected representative set of values of Δm^2 and $\sin^2 2\theta_V$. In the present article we have used the elliptical orbit approximation for the Earth motion around the Sun to calculate the one year average solar ν_e survival probability and the D-N asymmetry in the probability for neutrinos crossing the Earth mantle, the core, the inner 2/3 of the core, and the mantle + core. The indicated sampling which can be done with the Super - Kamiokande detector, was considered in order to investigate quantitatively the possibility of enhancement of the D-N effect. We have found, in particular, that such an enhancement can be especially large at small vacuum mixing angles, $\sin^2 2\theta_V \lesssim 0.013$: the D-N asymmetry in the one-year averaged ν_e survival probability for neutrinos crossing the Earth core only can be a factor of up to six bigger than the asymmetry in the analogous probability for neutrinos crossing the core + mantle (*Night* data sample). This result persists in the corresponding event rate samples [30], thus suggesting that it may be possible to test the $\sin^2 2\theta_V \leq 0.01$ region of the MSW solution of the solar neutrino problem by performing selective D-N asymmetry measurements with

the Super - Kamiokande detector.

We have studied also the accuracy of the circular orbit approximation (COA) utilized in many of the previous studies of the D-N effect, and compared it with the accuracy of the elliptical orbit approximation (EOA) we have used in the present analysis. The main conclusion of this study is that the largest difference in the results for the probability $\langle P_{e2} \rangle$ obtained using the COA and EOA is 0.8%. Given the fact that the EOA was chosen for the computations in this work, and that the EOA program actually includes most of the secondary celestial mechanics effects, the accuracy of the predictions for $\langle P_{e2} \rangle$ in what concerns the motion of the Sun is better (and probably much better) than 1%.

Acknowledgments

M.M. wishes to thank the International School for Advanced Studies, Trieste, Italy, where part of the work for this study has been done, for kind hospitality and financial support. The authors are indebted to the ICARUS group of the University of Pavia and INFN, Sezione di Pavia, and especially to Prof. E. Calligarich, for allowing the use of their computing facilities for the present study. M.M. wishes to thank also Dr. A. Rappoldi for his suggestions concerning the computational aspects of the study, and to Prof. A. Piazzoli for his constant interest in the work and support. The work of S.T.P. was supported in part by the EEC grant ERBFMRXCT960090 and by Grant PH-510 from the Bulgarian Science Foundation.

Appendix: The Solar Motion Approximations

The calculation of the probability $\langle P_{e2} \rangle$ with a sufficient accuracy requires a relatively good approximation for the Sun's apparent motion which to leading order can be considered as a superposition of two strictly periodical motions, the orbital revolution and the Earth rotation, plus a set of small perturbations. The exact solution of such perturbation problem is complex and computationally demanding and therefore one has to select only those effects which are relevant for the chosen accuracy threshold ϵ (ref. [27, 34, 35, 36]). The various errors introduced by inadequate approximations are systematic in nature. They combine algebraically leading to subtle cancelation or enhancement effects which are difficult to propagate to the probability $\langle P_{e2} \rangle$ of interest. However, a practical approach to cut off all corrections which are not relevant is to set a threshold in the Sun's motion tracking accuracy of the order of some arcmin. This threshold may be justified by the fact that the Sun is not a point like neutrino source and the neutrino production region has an apparent angular diameter of about 3 arcmin (approximately one tenth of the solar diameter). The correctness of the indicated choice is confirmed by a more detailed analysis.

Using the accuracy threshold it is possible to discriminate between the various assumptions which can be used to simplify the apparent solar motion. As a result of such an analysis it becomes evident that two orbital approximations are sufficiently accurate for our purposes: the circular orbit approximation (COA) and the Elliptical Orbit Approximation (EOA). In the COA the Sun's orbit is circular, while in the EOA the true elliptical Sun's orbit described by Kepler's laws is considered. There are two important effects which are neglected by COA and which instead are included in EOA: i) the time dependence

of the Sun - Earth distance, $R(t)$, during the year, which leads to a change in the solar neutrino flux at the Earth, Φ , according to the $1/R^2(t)$ law, ii) the time dependence of the Earth orbital velocity, $v(t)_{\oplus}$, during the year due to the angular momentum conservation. The velocity $v(t)_{\oplus}$ also changes according to the $1/R^2(t)$ law. This implies a change in the residence time of the Earth, $T_{res,\oplus}$, in a given orbital location, which is proportional to $R^2(t)$. Each of these two effects can introduce a systematic error of up to 3%. When taken together into account they compensate partially each other because the total neutrino rate for a given position of the Earth with respect to the Sun is proportional to the product $T_{res,\oplus}\Phi$ and therefore the total effect has to be rather small for a one year average *Night* sample. However, when other samples as *Core* or *Deep - Core* are considered cancelation at the 1% level cannot be guaranteed by pure heuristic arguments since even with an one year data taking the *Core* and *Deep - Core* sampling are equivalent to averaging over a fraction of the year (winter). In addition, for detectors located at positive latitudes over the tropical band, the *Core* sample is detected at winter when Φ_{\odot} and $v(t)_{\oplus}$ are maximal.

For the aforementioned reasons a set of numerical simulations were performed using both COA and EOA approximations and comparing the results for both $\langle P_{e2} \rangle$ and T_{res} obtained with them. As already stated in the text, the main conclusion of this study is that the largest difference in the results for $\langle P_{e2} \rangle$ obtained utilizing the COA and EOA is 0.8%, and that the 3 arcmin error threshold provides a sufficient accuracy in the description of the solar motion. Let us note also that the program which make use of the elliptical orbit approximation takes into account many other celestial mechanics secondary effects as well, so that its accuracy is better than few tenth of an arcmin. Since all the results presented in this paper are obtained with this program, it is evident that the accuracy of $\langle P_{e2} \rangle$ predictions here presented is far better than 1%.

A number of tests were also performed to assure that the accuracy of the numerical calculations is sufficiently high. For instance, calculated solar positions were compared with positions given in the 1996 edition of the *Nautical Almanac* [36]. These tests showed that the numerical errors are not greater than $10^{-3}\%$ and therefore are negligible.

Finally, let us note that eq. (8) can also be written using the ratio

$$\frac{1}{T_{res}(\hat{h} \leq 90^\circ)} \frac{dT_{res}}{d\hat{h}} ,$$

i.e., the probability to receive a neutrino from the Sun (of any flavour or energy) when it is inside the Nadir angle interval $\hat{h}, \hat{h} + d\hat{h}$. In this case the expression for the average transition probability for the Nadir angle interval $[\hat{h}_1, \hat{h}_2]$ becomes:

$$\langle P_{e2} \rangle = \int_{\hat{h}_1}^{\hat{h}_2} d\hat{h} P_{e2}(\hat{h}) \frac{1}{T_{res}(90^\circ)} \frac{dT_{res}}{d\hat{h}} . \quad (\text{A.1})$$

Although it looks more attractive theoretically, this formulation is unpractical due to the presence of 365 singularity points in the $dT_{res}/d\hat{h}$ function, as is illustrated in Fig. 4. These singularities are due to the fact that when the Sun's Nadir angle reaches its minimum value, $d\hat{h}(t)/dt$ vanishes while $dT_{res}/d\hat{h} \approx 1/(d\hat{h}(t)/dt)$ diverges. Obviously, these singularities are integrable but they make rather complicated the use of eq. (A.1) for sufficiently accurate calculations.

Tables

Table I. List of the Δm^2 and $\sin^2 2\theta$ sample values

$\sin^2 2\theta_V$	$\Delta m^2(\text{eV}^2)$			
	I	II	III	IV
0.0008	9E-6	7E-6	5E-6	
0.0010	9E-5	7E-6	5E-6	
0.0020	1E-5	7E-6	5E-6	
0.0040	1E-5	7E-6	5E-6	
0.0060	1E-5	7E-6	5E-6	
0.0080	1E-5	7E-6	5E-6	
0.0100	7E-6	5E-6		
0.0130	5E-6			
0.3000	1.5E-5	2.0E-5	3.0E-5	4.0E-5
0.4800	3E-5	5E-5		
0.5000	2E-5			
0.560	1E-5			
0.600	8E-5			
0.700	3E-5	5e-5		
0.770	2E-5			
0.800	1.3E-4			
0.900				

Table II. Residence times for the Super - Kamiokande detector.

Sample s	Nadir Angle \hat{h}		$\frac{T_{res}^s}{T_y} \times 100$	$\frac{T_{res}^s}{T_{res}^N} \times 100$	$\frac{\sigma(\mathcal{R}_E)}{\mathcal{R}_E} \times 100$
	from	to			
<i>Deep - Core</i>	0°	25.98°	3.94	7.86	5.0
<i>Core</i>	0°	33.17°	7.11	14.18	3.8
<i>Mantle</i>	33.17°	90°	43.03	85.82	1.5
<i>Night</i>	0°	90°	50.14	-	1.4

Note:

$T_y = 365.243$ days.

The integration is extended over one year from day 0 to day 365

$\sigma(\mathcal{R}_E)$ is the 1 year mean event rate statistical uncertainty for $\mathcal{R}_{E,0} = 10^4 \nu/\text{year}$

References

- [1] S.P. Mikheyev and A.Yu. Smirnow, Sov. J. Nucl. Phys. **6**, 913 (1985); L. Wolfenstein, Phys. Rev. D **20**, 2369 (1978).
- [2] P.I. Krastev and S.T. Petcov, Reported by S.T. Petcov at the “Neutrino’96” International Conference on Neutrino Physics and Astrophysics, June 13-19, 1996, Helsinki, Finland.
- [3] J.N. Bahcall and M.H. Pinsonneault, Rev. Mod. Phys. **67**, 781 (1995)
- [4] J.N. Bahcall et al., Preprint in: <http://babbage.sissa.it>, astro-ph/9610250 (1996)
- [5] P.I. Krastev and A.Yu. Smirnov, Phys. Lett. B **338**, 282 (1994); V. Berezinsky. G. Fiorentini and M. Lissia, *ibid.* B**341**, 38 (1994); N. Hata and P. Langacker, Phys. Rev. D**52**, 420 (1995).
- [6] M. Cribier et al., Phys. Lett. B **182**, 89 (1986); J. Bouchez et al., Z. Phys. C **32**, 499 (1986).
- [7] S.P. Mikheyev and A.Yu. Smirnov, in *New and Exotic Phenomena*, Proceedings of the Moriond Workshop, Les Arcs, Savoie, France, 1987, edited by O. Fackler and J. Tran Thanh Van (Editions Frontières, Gif-sur-Yvette, France, 1987), p. 405.
- [8] E.D. Carlson, Phys. Rev. D **34**, 1454 (1986).
- [9] S. Hiroi et al., Prog. Theor. Phys. **78**, 1433 (1987).
- [10] A.J. Baltz and J. Weneser, Phys. Rev. D **35**, 528 (1987); *ibid.* D **37**, 3364 (1988).
- [11] A. Dar and A. Mann, Nature **325**, 790 (1987).
- [12] A.J. Baltz and J. Weneser, Phys. Rev. D **50**, 5971 (1994).
- [13] N. Hata and P. Langacker, Phys. Rev. D **50**, 632 (1994)
- [14] P.I. Krastev, Preprint in: <http://www.babbage.sissa.it>, hep-ph/9610339 (1996)
- [15] J.M. Gelb, W. Kwong and S.P. Rosen, Preprint in: <http://www.babbage.sissa.it>, hep-ph/9612332 (1996).
- [16] K.S. Hirata, et al., Phys. Rev. D **44**, 2241 (1991); K.S. Hirata, et al., Phys. Rev. Lett. **66**, 9 (1991); Y. Fukuda et al., Phys. Rev. Lett. **77**, (1996) 1683.
- [17] V.K. Ermilova, V.A. Tsarev and V.A. Chechin, JETP Letters **43**, 453 (1986).
- [18] J.M. LoSecco, Phys. Rev. D **47**, 2032 (1993).
- [19] P.I. Krastev and S.T. Petcov, Phys. Lett. B **207**, 64 (1988).
- [20] A. Dar et al., Phys. Rev. D **35**, 3607 (1987).
- [21] A. Nicolaidis, Phys. Lett. B **200**, 553 (1988).
- [22] B. Bertotti and M. Maris, *Variabilità Temporale del Flusso di Neutrini Solari in Esperimenti Sotterranei (Neutrino Flux Time Variability in Underground Experiments)*, 1996, reported in the Ph.D. thesis of M. Maris, Department of Theoretical and Nuclear Physics (D.F.N.T.), Pavia University, Italy, in Italian.

- [23] F.D. Stacey, *Physics of the Earth, 2nd edition*, John Wiley and Sons, London, New York, 1977.
- [24] R. Jeanloz, *Annu. Rev. Earth Planet. Sci.* **18**, 356 (1990).
- [25] S.T. Petcov, *Phys. Lett. B* **200**, 373 (1988).
- [26] P.I. Krastev and S.T. Petcov, *Phys. Lett. B* **205**, 84 (1988).
- [27] K.R. Lang, *Astrophysical Formulae, 2nd edition*, Springer - Verlag, Heilderberg, 1980.
- [28] J.N. Bahcall, M. Kamionkowski and A. Sirlin, *Phys. Rev. D* **51**, 6146 (1995).
- [29] Y. Suzuki, Private communication (1996).
- [30] M. Maris and S.T. Petcov, SISSA Report ref. SISSA 17/97/EP, January 1997.
- [31] V. Barger et al., *Phys. Rev. D* **17**, 2718 (1980); P. Langacker et al., *ibid.* **D 27**, 1228 (1983).
- [32] T.K. Kuo and J. Pantaleone, *Rev. of Mod. Phy.* **61**, 937 (1989).
- [33] W.H. Press, B.P. Flannery, S.A. Teukolsky, W.T. Vetterling, *Numerical Recipes*, Cambridge University Press, Cambridge, 1986.
- [34] F. Zagar, *Astronomia Sferica e Teorica (Spherical and Theoretical Astronomy)*, Zanichelli, Bologna, 1984.
- [35] O. Montembruck, T. PFleger, *Astronomy on the Personal Computer*, Springer - Verlag, Berlin, Heidelberg, 1989.
- [36] *The Nautical Almanac*, Edited by the Nautical Almanac Office, Washington USA (1996).

Figure Captions

Figure 1. The geometry of the Earth effect: D and \odot denote the detector and the Sun, \hat{h} is the Sun's Nadir angle, R_{\oplus} is the Earth radius (6371 km) and R_{core} is the core radius (3486 km). The small arrows point in the directions of the detector Zenith and Nadir.

Figure 2. The dependence of the probability P_{e2} on ρ_R for $\sin^2 2\theta_V = 0.01$. The five plots are obtained for $0.1 \text{ gr/cm}^3 \leq \rho_R \leq 30.0 \text{ gr/cm}^3$ and five different solar neutrino trajectories in the Earth: a) center crossing ($\hat{h} = 0^\circ$), b) winter solstice for the Super - Kamiokande detector ($\hat{h} = 13^\circ$), c) half core for the Super - Kamiokande detector ($\hat{h} = 23^\circ$), d) core/mantle boundary ($\hat{h} = 33^\circ$), e) half mantle ($\hat{h} = 51^\circ$).

Figure 3. The probabilities $\langle P_{e2} \rangle$ and P_{\oplus} as functions of $E/\Delta m^2$. Each figure represents \bar{P}_{\odot} , $\langle P_{e2} \rangle$, P_{\oplus} and \mathcal{A}_P for the value of $\sin^2 2\theta_V$ indicated in the figure. The frames (a) show the probability $\langle P_{e2} \rangle$ as a function of the resonance density ρ_R for the *Night* (*short - dashed Line*), *Mantle* (*dotted line*), *Core* (*full line*) and *Deep - Core* (*long - dashed line*) samples. The frames (b), (c) and (d) represent the probabilities \bar{P}_{\odot} (*Dotted Line*), $\langle P_{e2} \rangle$ (*Dashed Line*), P_{\oplus} (*Full Line*) corresponding to the *Night*, *Core* and *Mantle* samples as functions of $E_{\nu}/\Delta m^2$. In some cases $\langle P_{e2} \rangle$ is multiplied by a factor of 10, which is indicated in the corresponding figures.

Figure 4. Distribution of the differential residence time $dT_{res}/d\hat{h}^\circ$ for the Super - Kamiokande detector. The Nadir angle is expressed in degrees. The upper figure depicts the distribution for $\hat{h} \leq 89^\circ$, while the lower figure shows an enlargement of the distribution for $40^\circ \leq \hat{h} \leq 44^\circ$. The lower figure shows also that the small wiggles in the upper figure are due to a set of singularities not well sampled by the computing algorithm. The peaks in the lower figure have a finite height only because of limitations in the numerical computation accuracy.

Figure 1

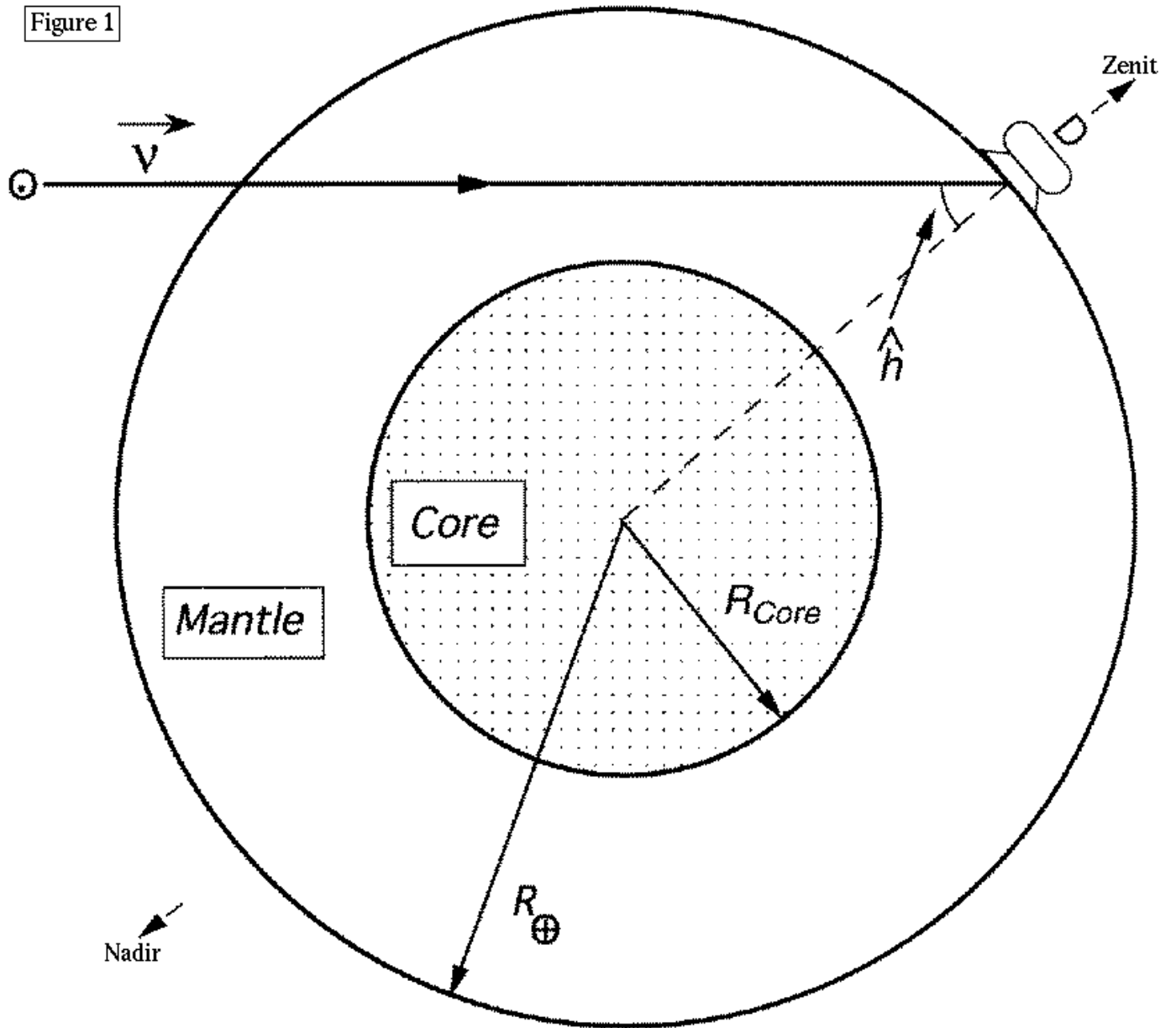


Figure 3.1 $\sin^2(2\theta_{\nu}) = 0.0008$

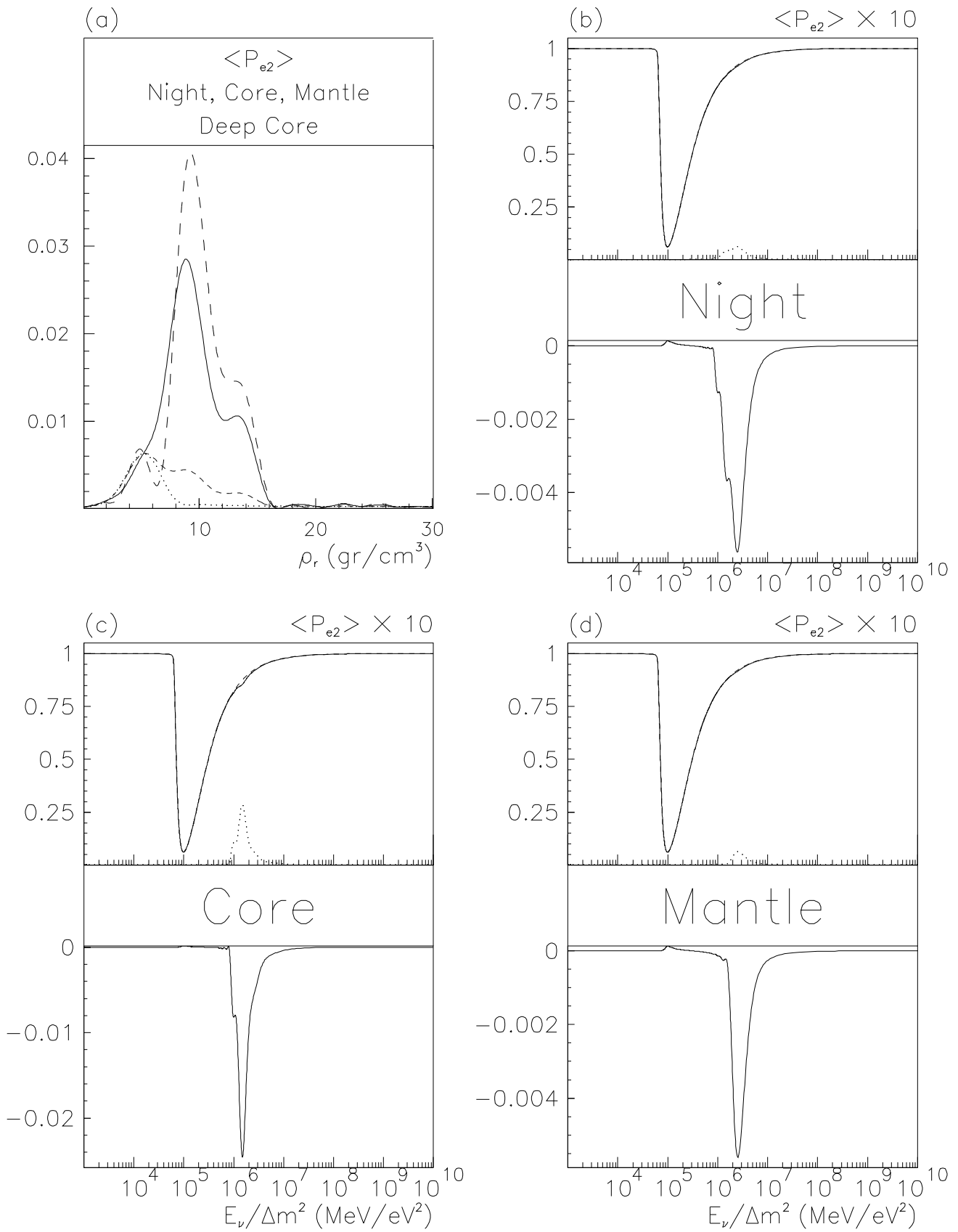


Figure 2

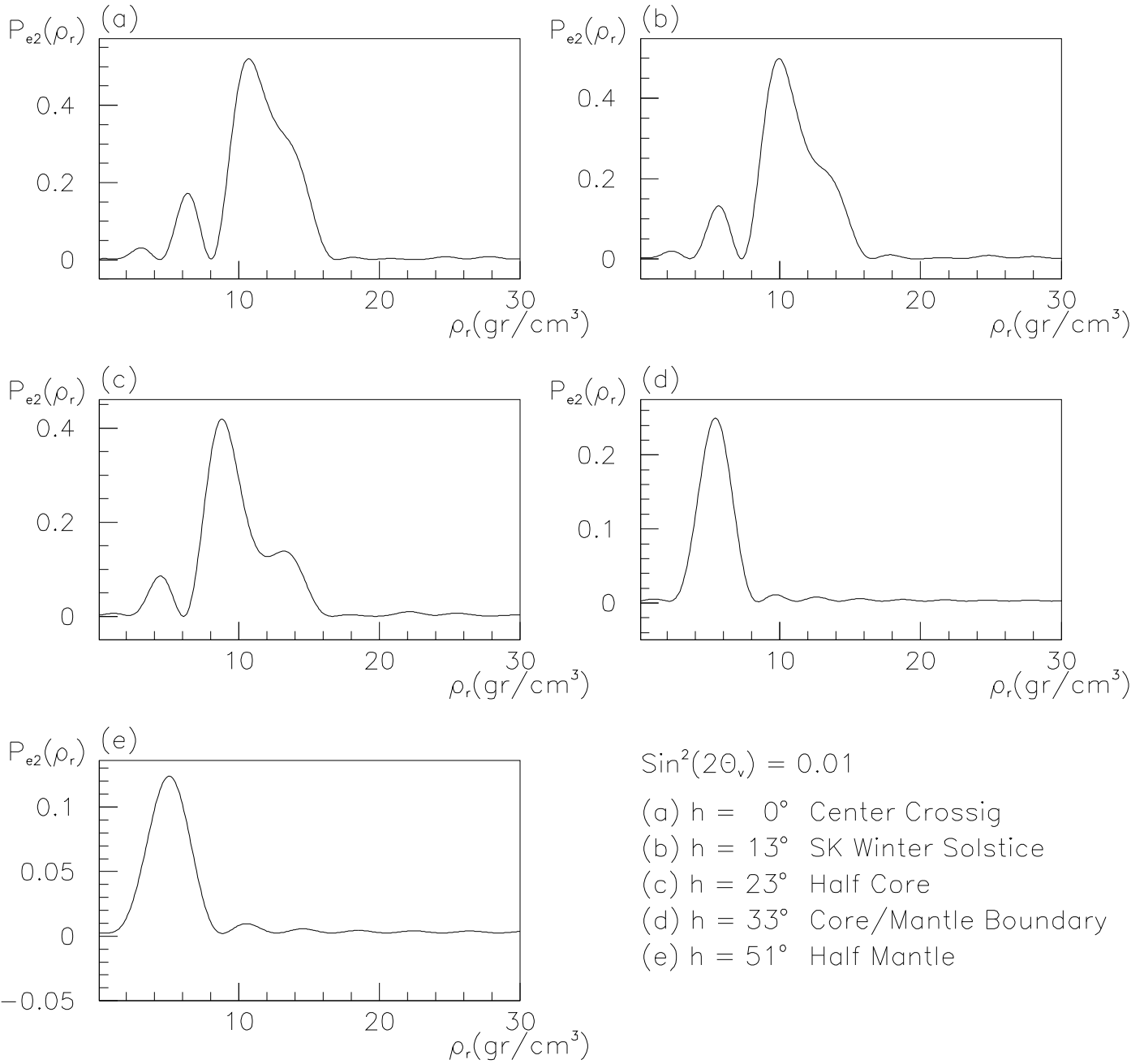


Figure 3.2 $\sin^2(2\theta_{\nu}) = 0.0010$

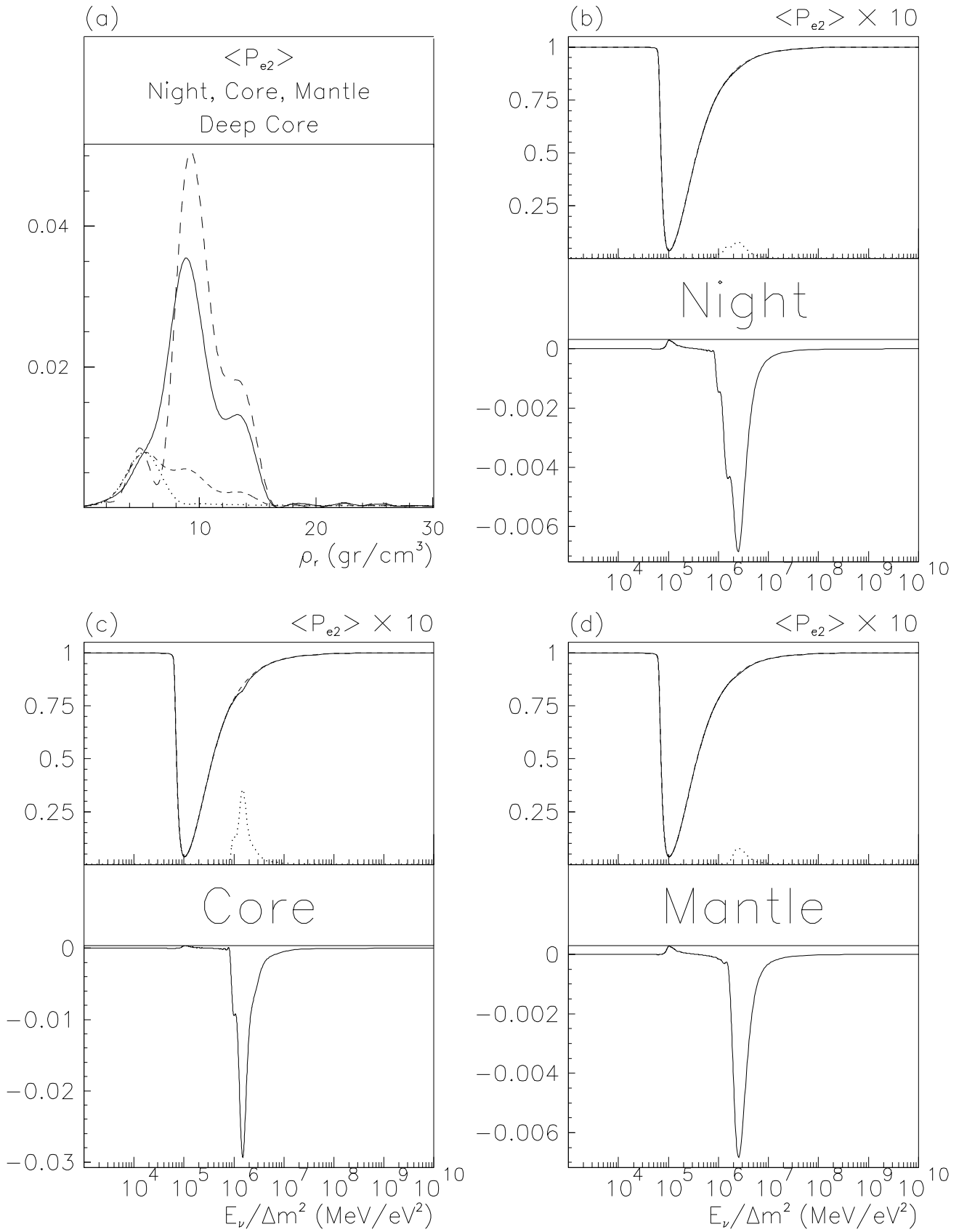
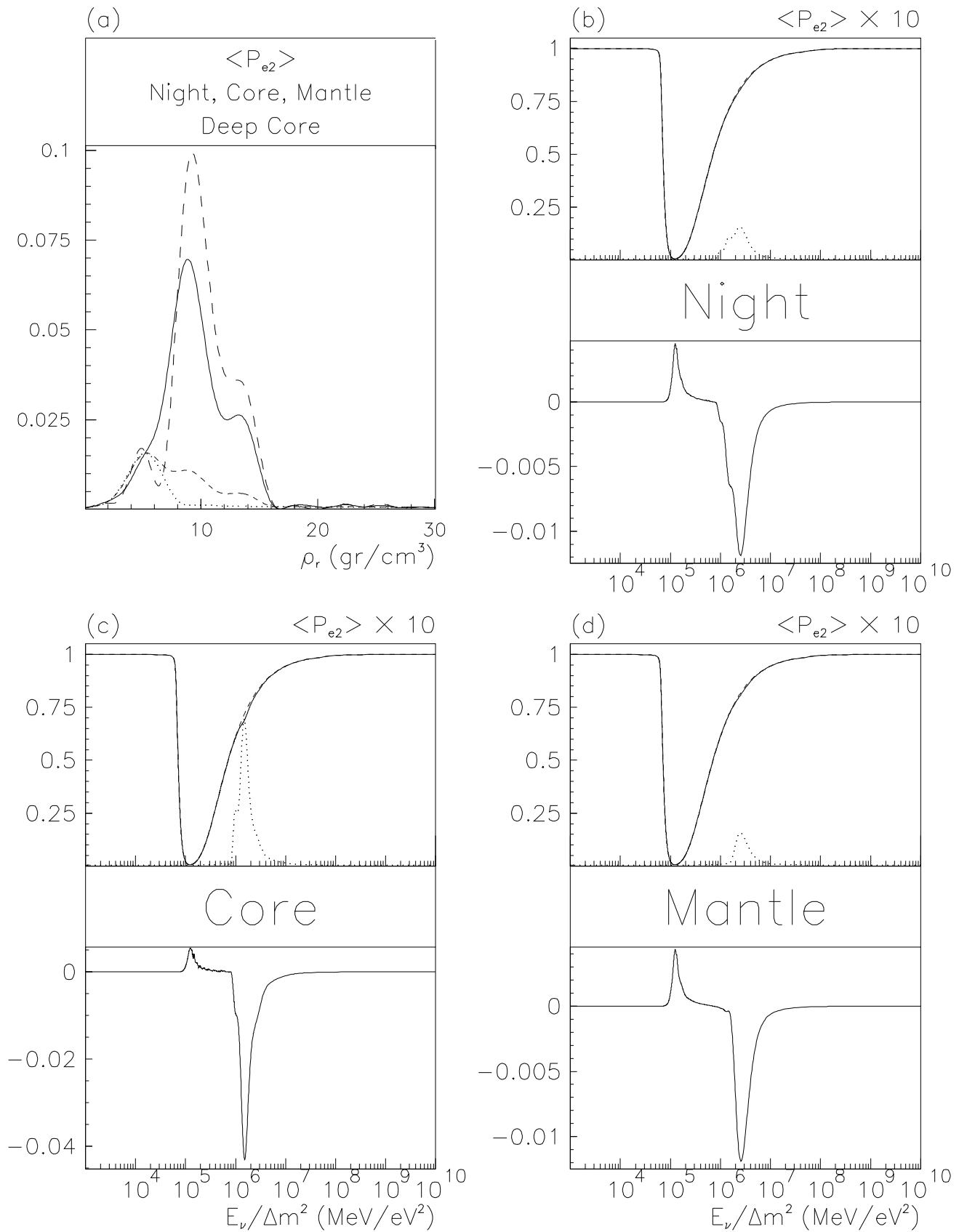


Figure 3.3 $\sin^2(2\theta_\nu) = 0.0020$



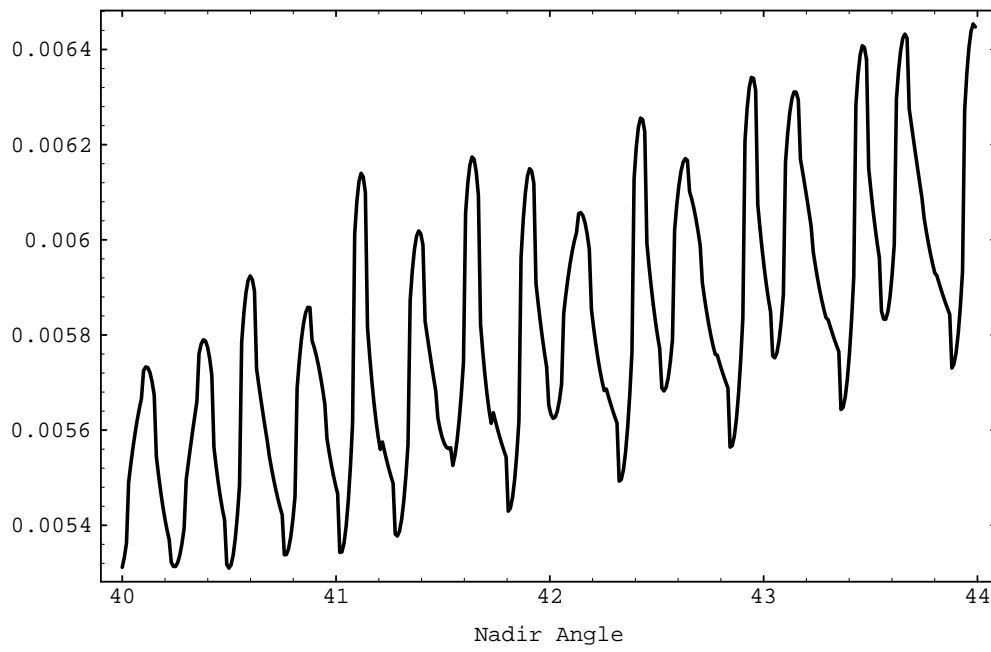
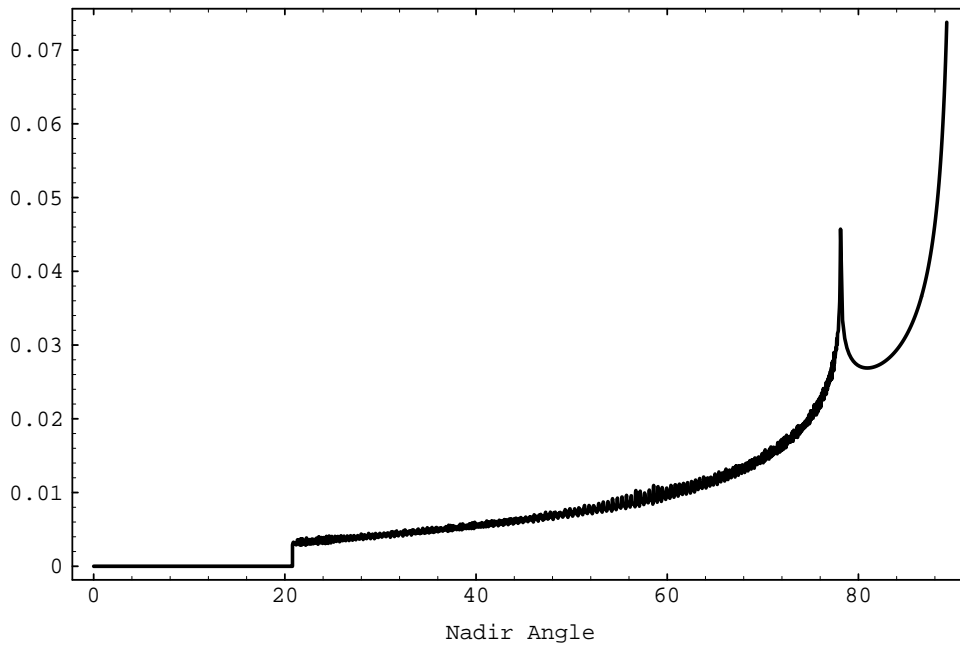


Figure 4

Figure 3.4 $\sin^2(2\theta_{\nu}) = 0.0040$

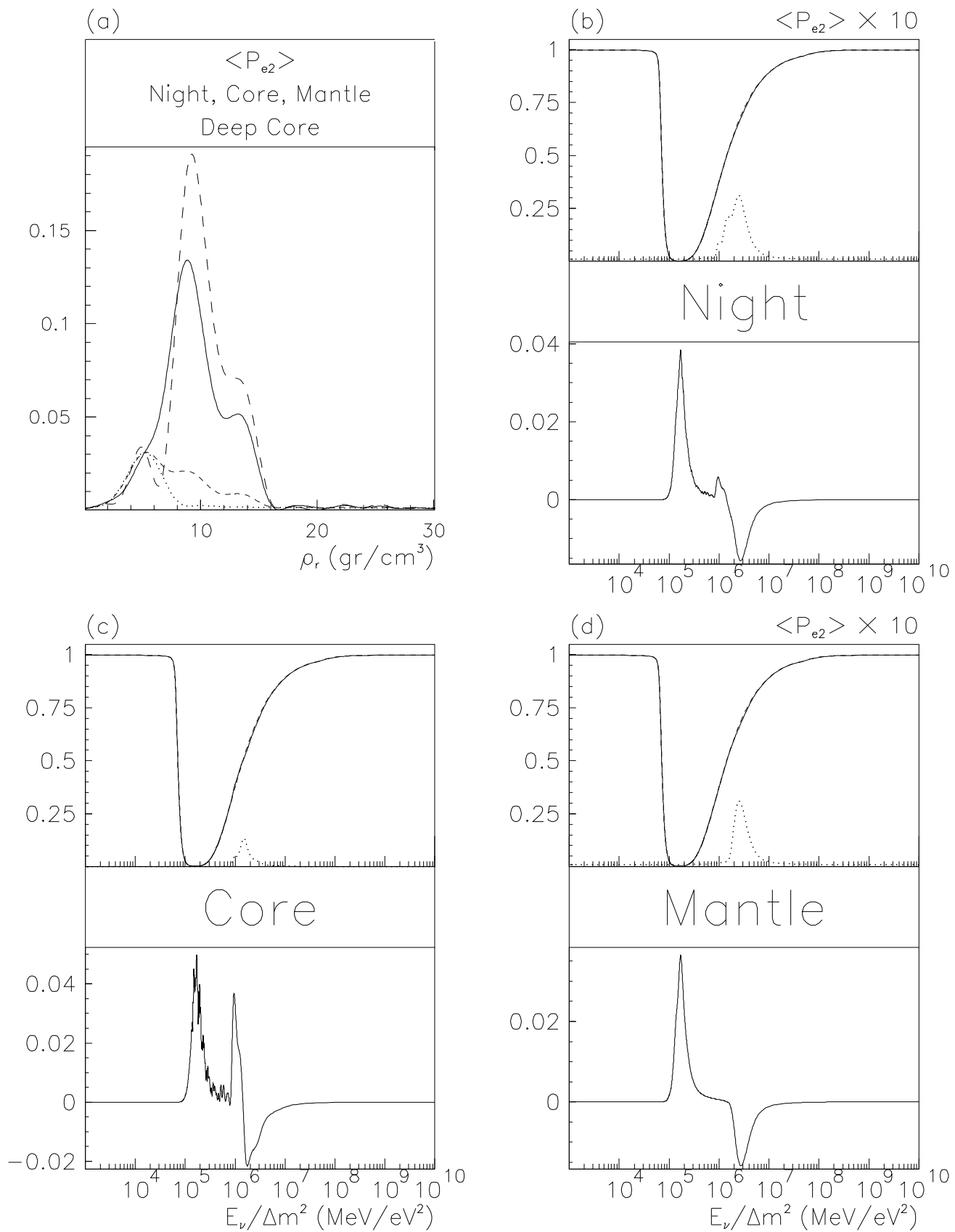


Figure 3.5 $\sin^2(2\theta_{\nu}) = 0.0060$

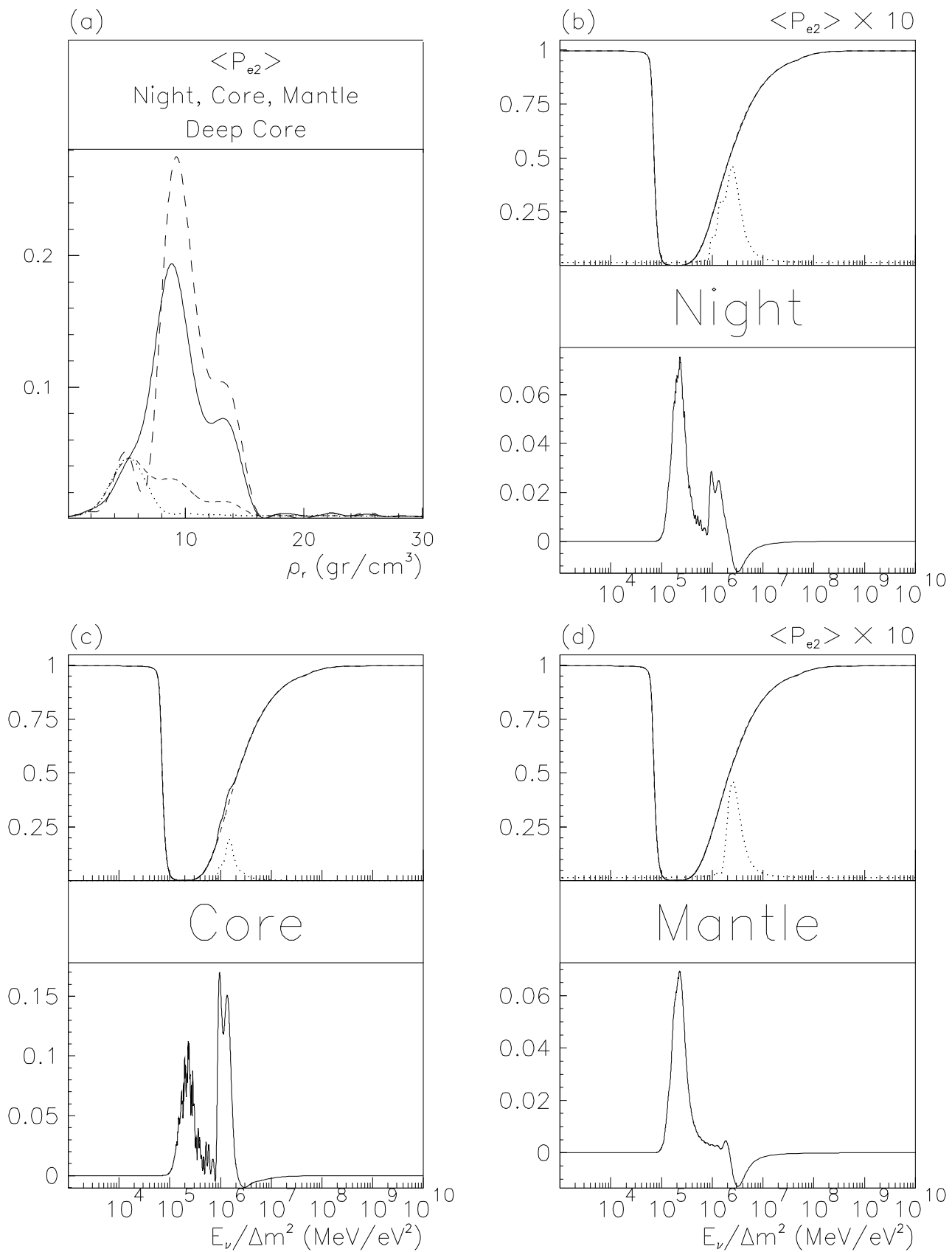


Figure 3.6 $\sin^2(2\theta_{\nu}) = 0.0080$

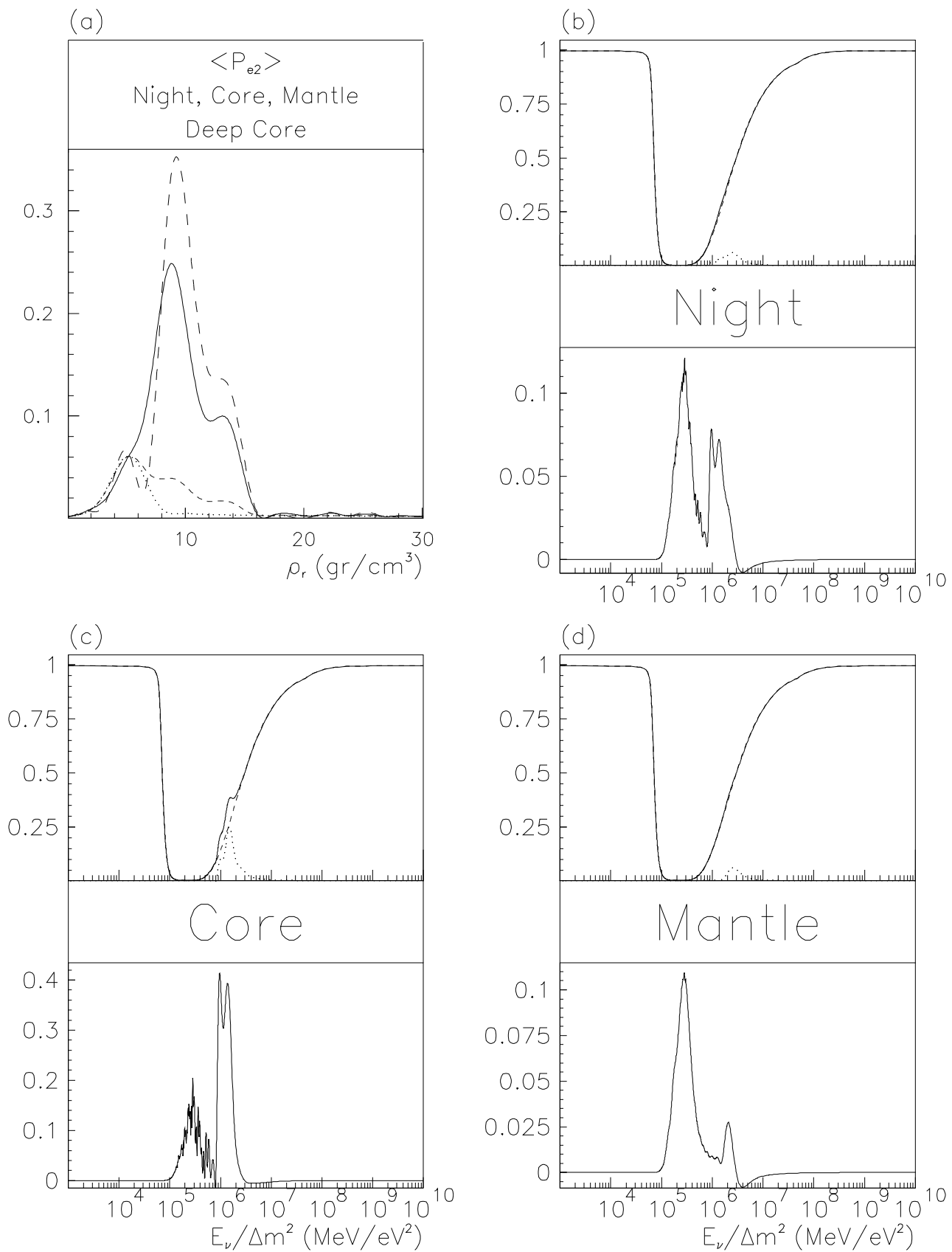


Figure 3.7 $\sin^2(2\theta_{\nu}) = 0.010$

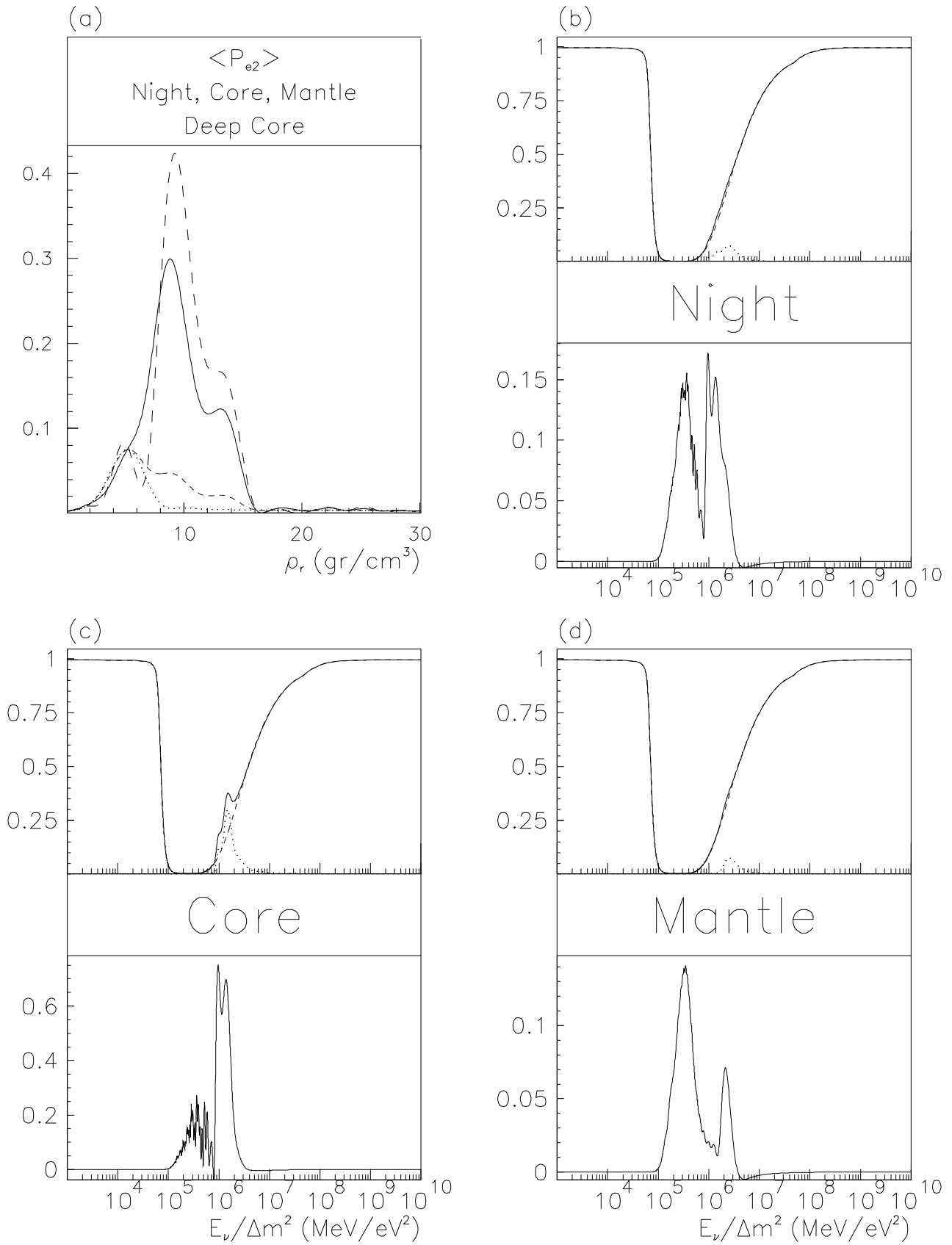


Figure 3.8 $\sin^2(2\theta_{\nu}) = 0.0130$

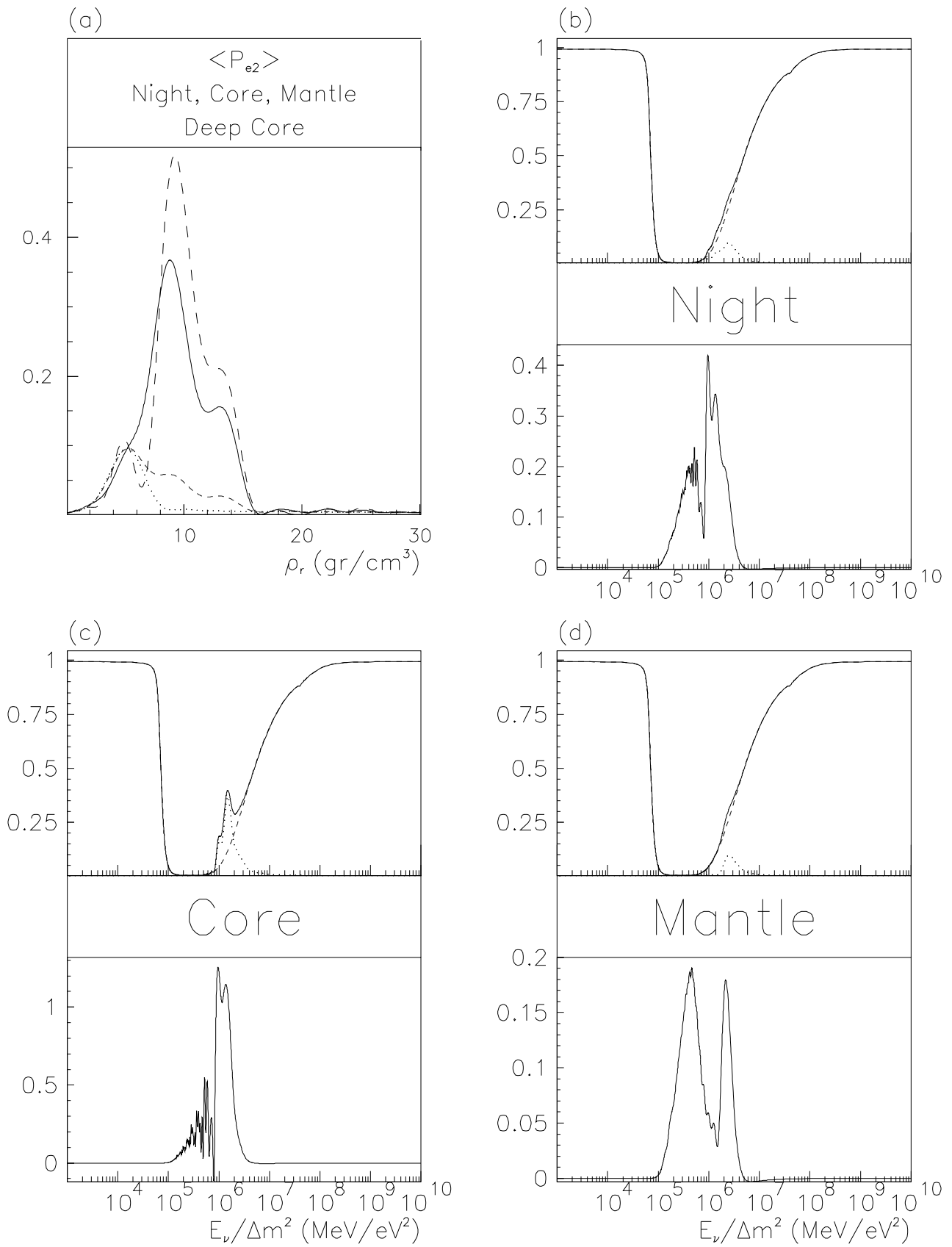


Figure 3.9 $\sin^2(2\theta_{\nu}) = 0.030$

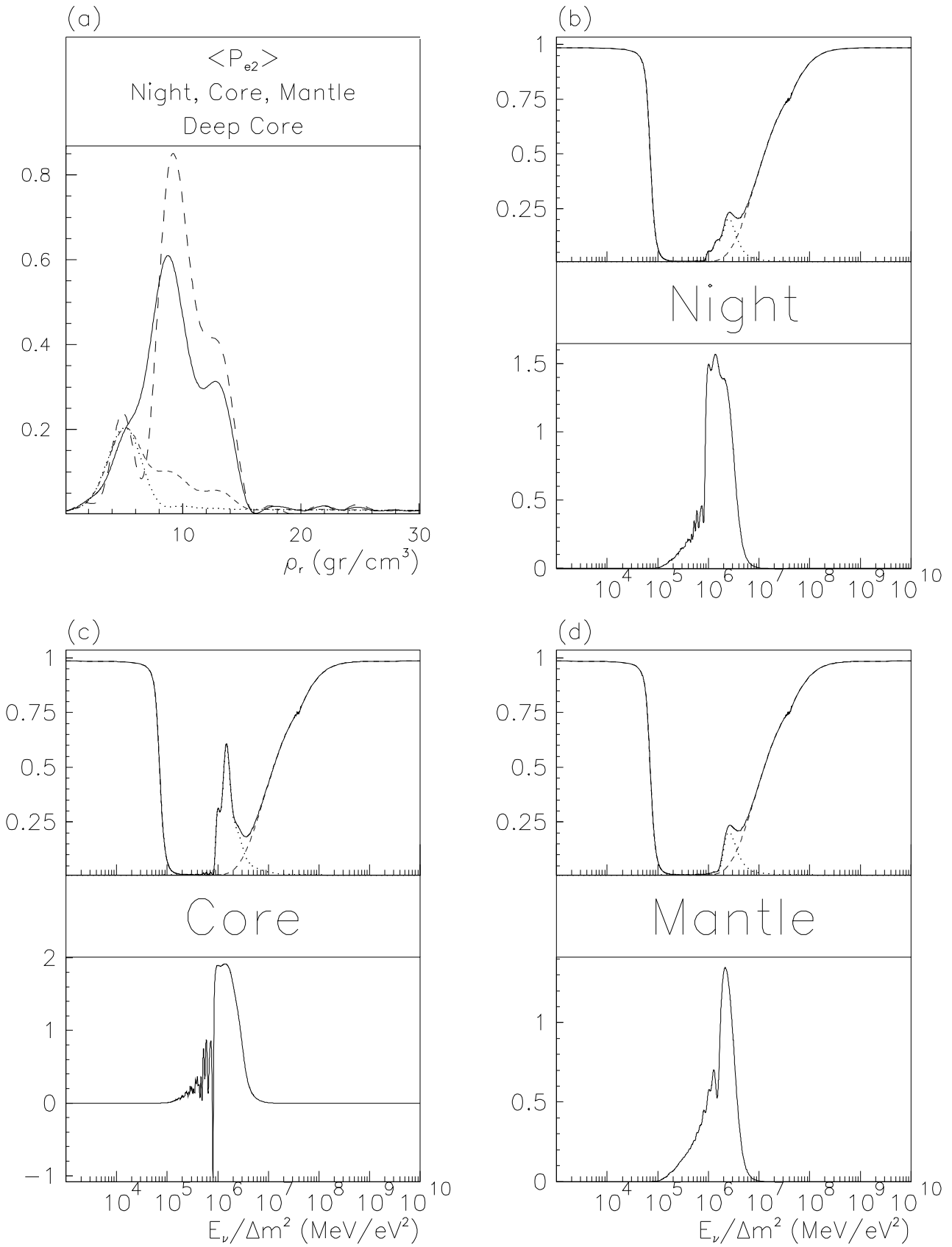


Figure 3.10 $\sin^2(2\theta_\nu) = 0.300$

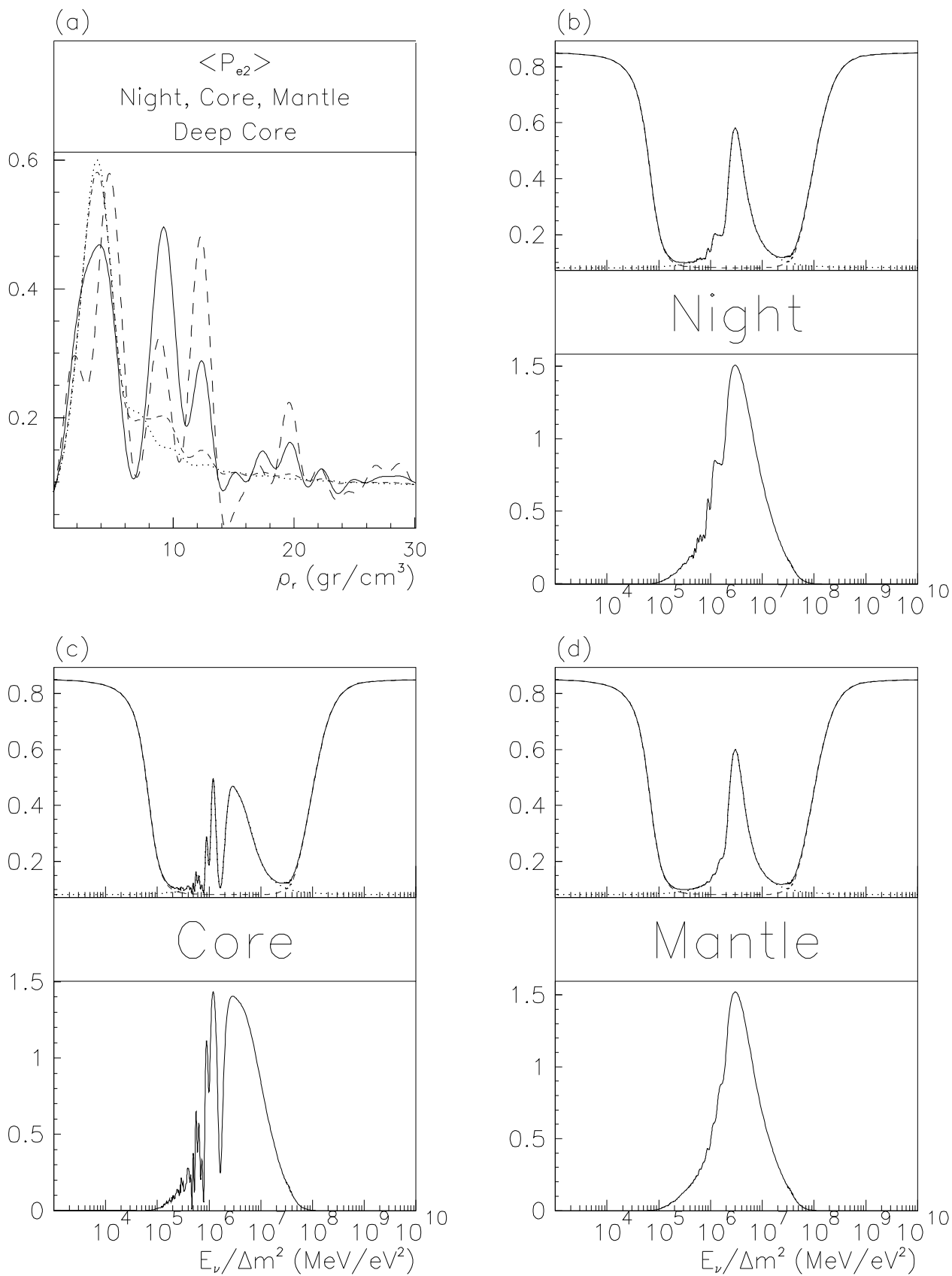


Figure 3.11 $\sin^2(2\theta_\nu) = 0.480$

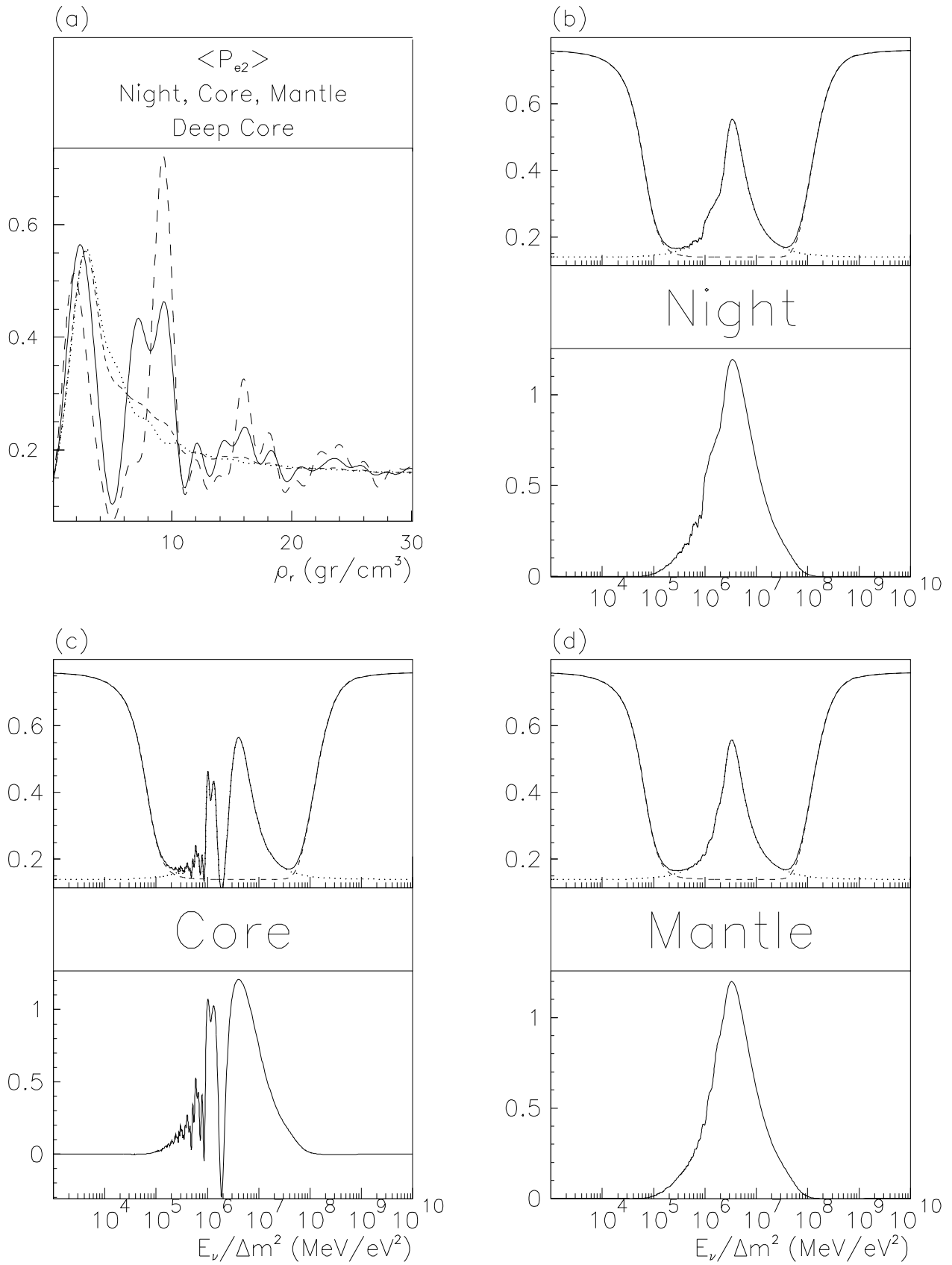


Figure 3.12 $\sin^2(2\theta_\nu) = 0.500$

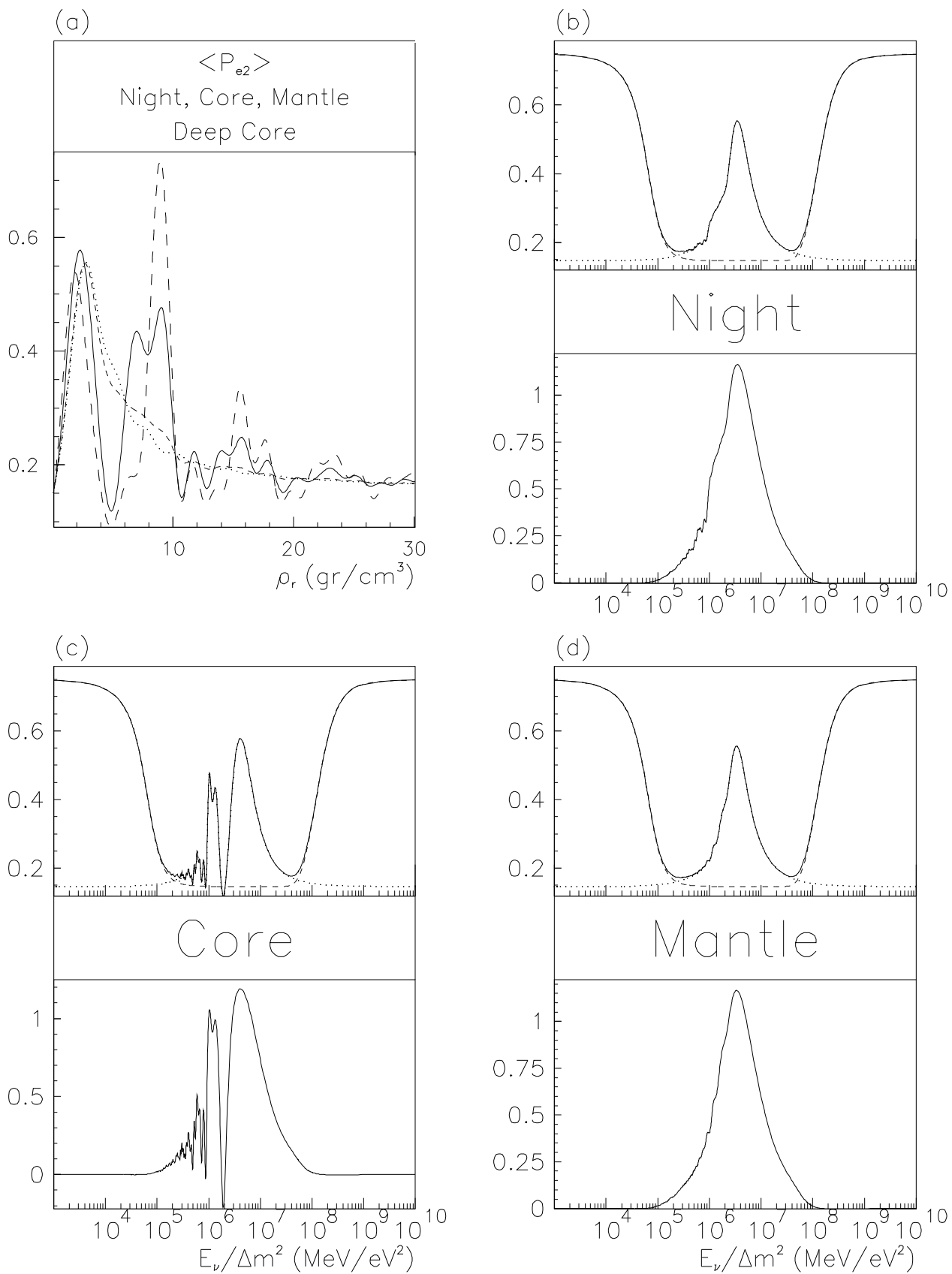


Figure 3.13 $\sin^2(2\theta_{\nu}) = 0.560$

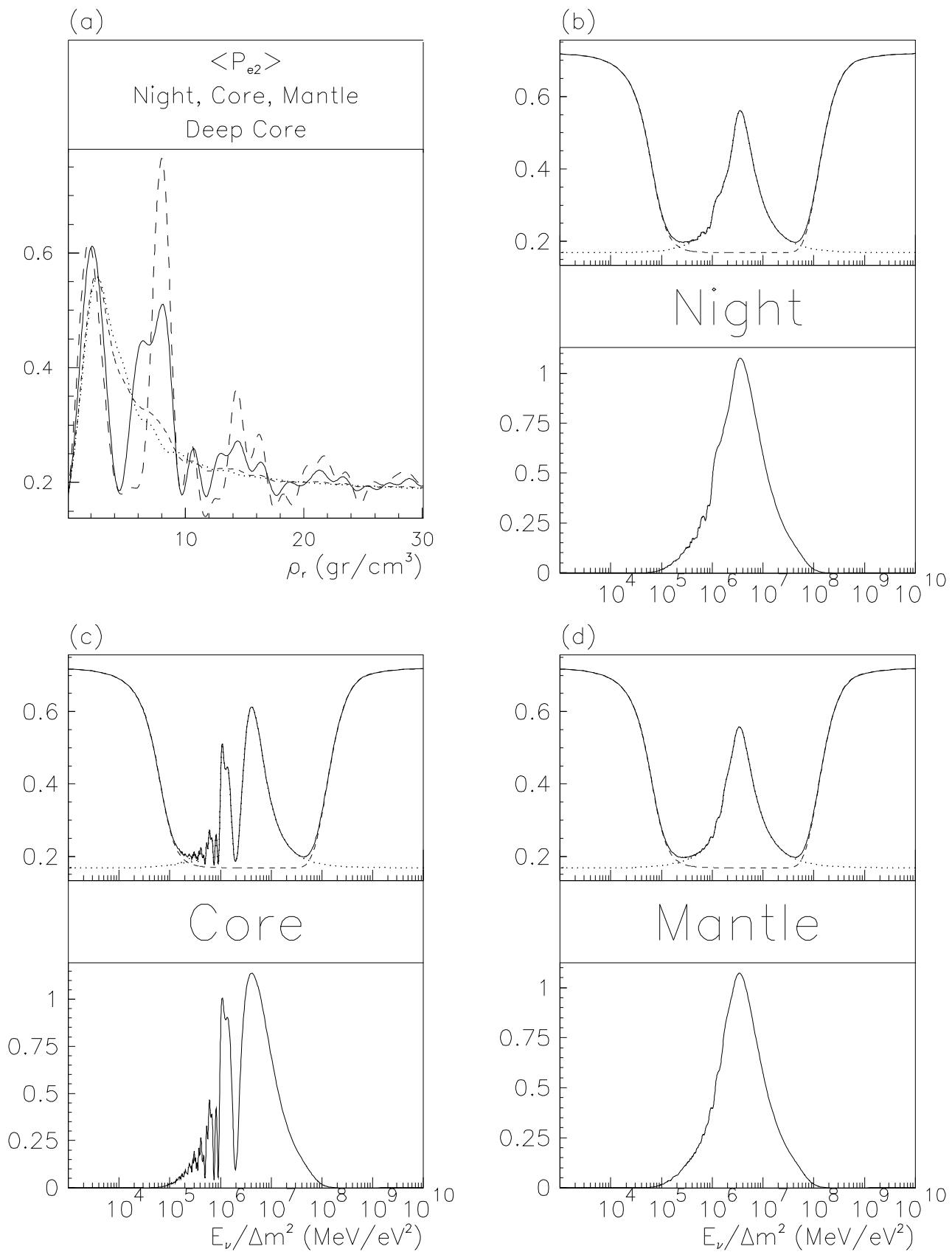


Figure 3.14 $\sin^2(2\theta_\nu) = 0.600$

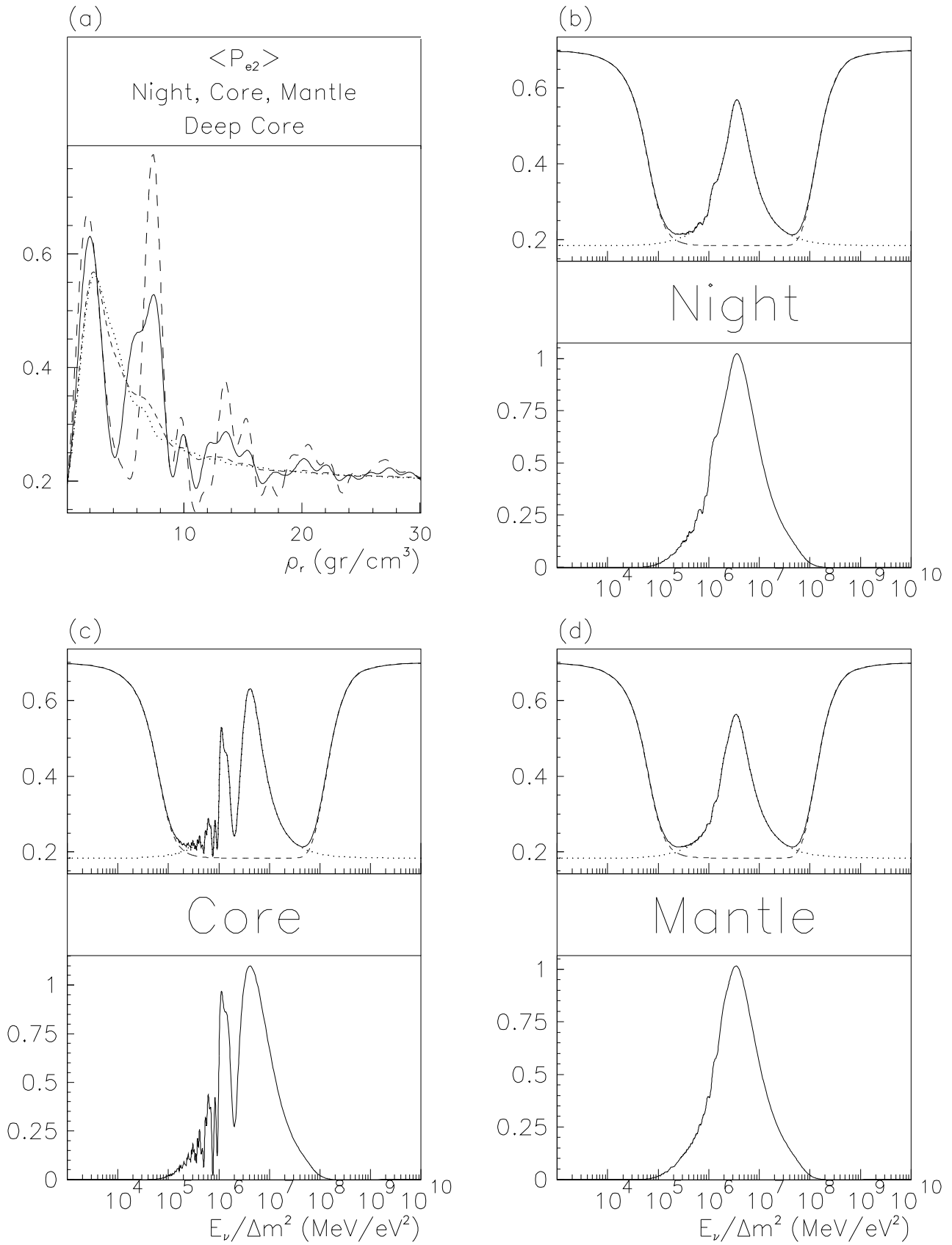


Figure 3.15 $\sin^2(2\theta_{\nu}) = 0.700$

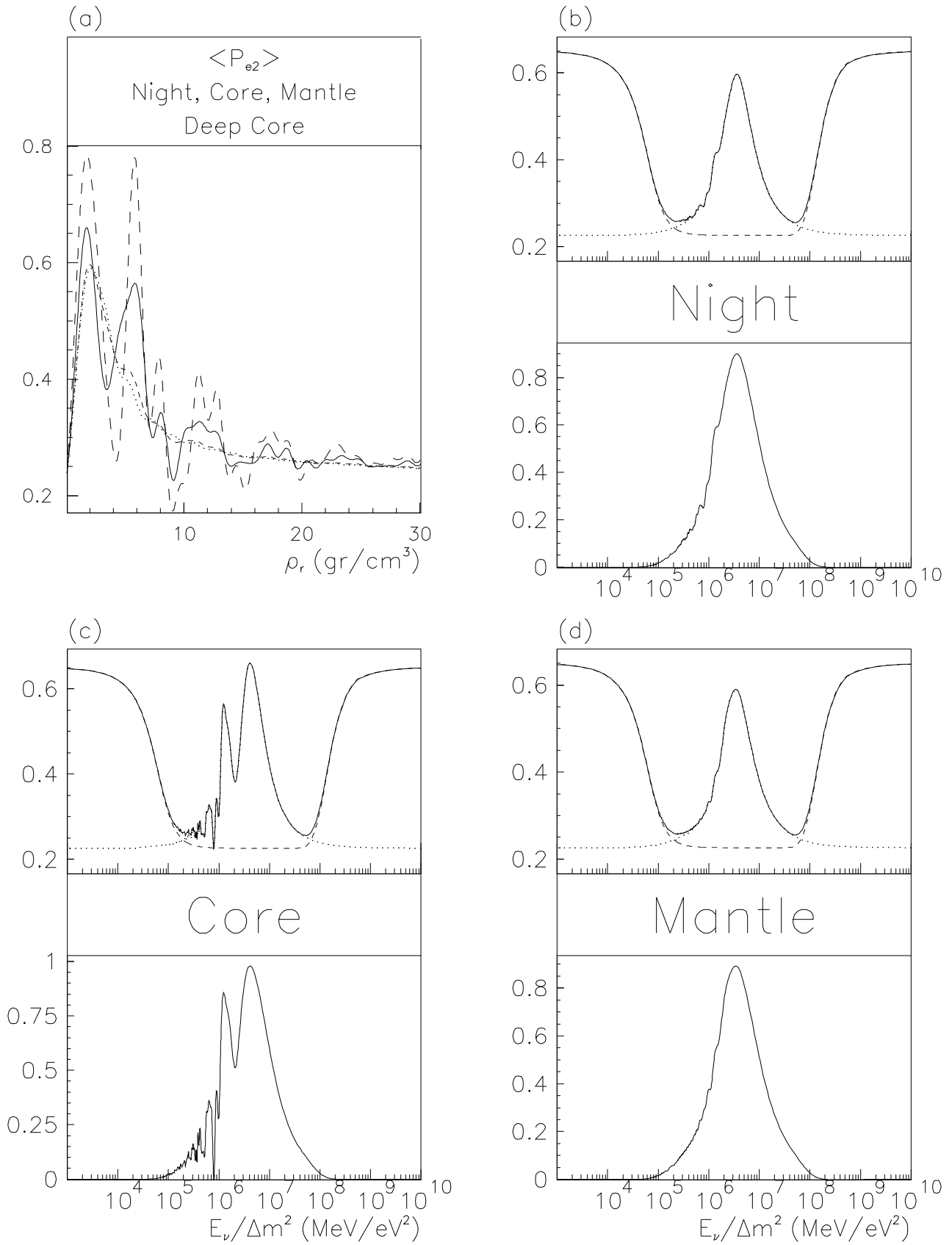


Figure 3.16 $\sin^2(2\theta_{\nu}) = 0.770$

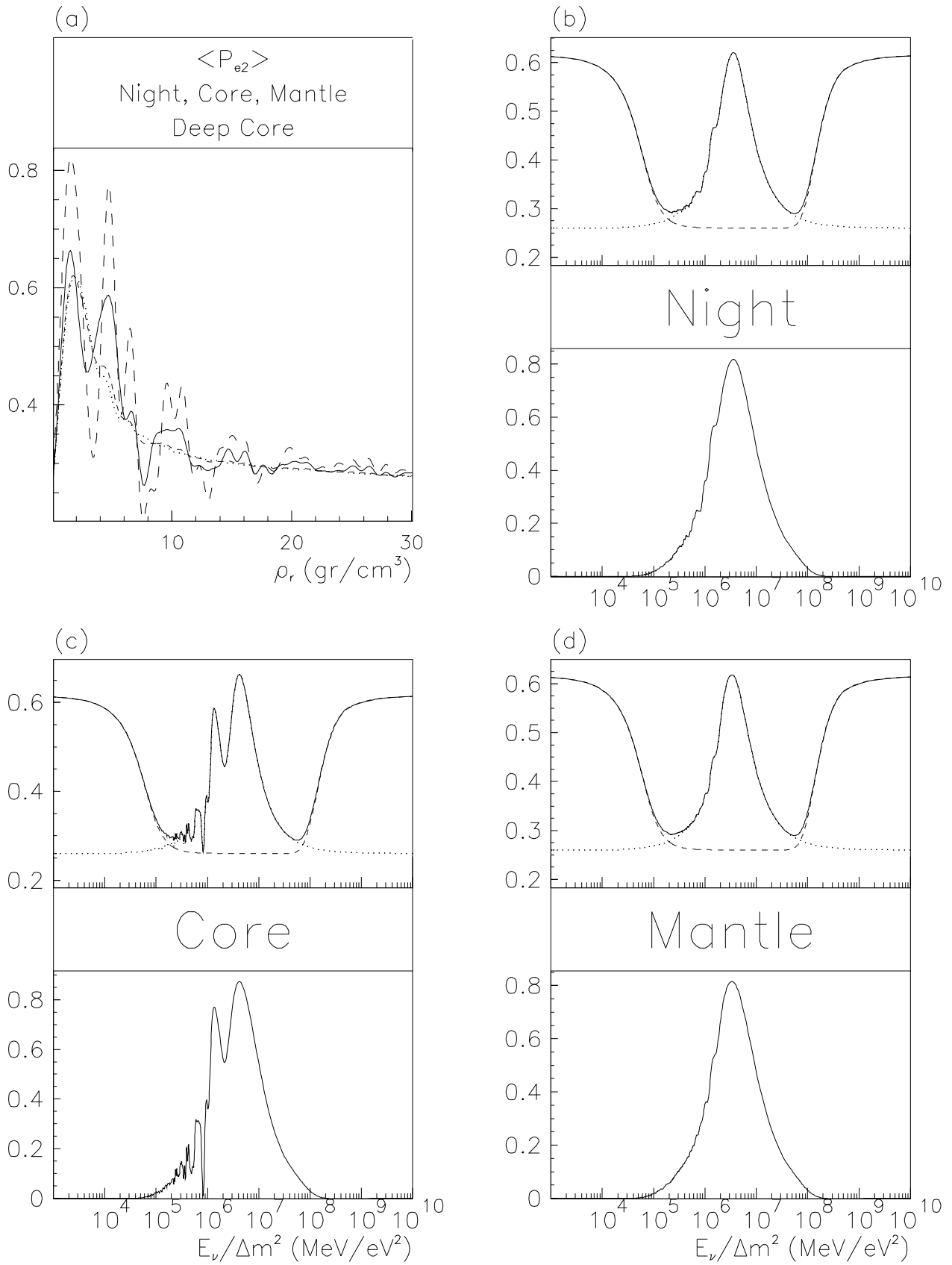


Figure 3.17 $\sin^2(2\theta_\nu) = 0.800$

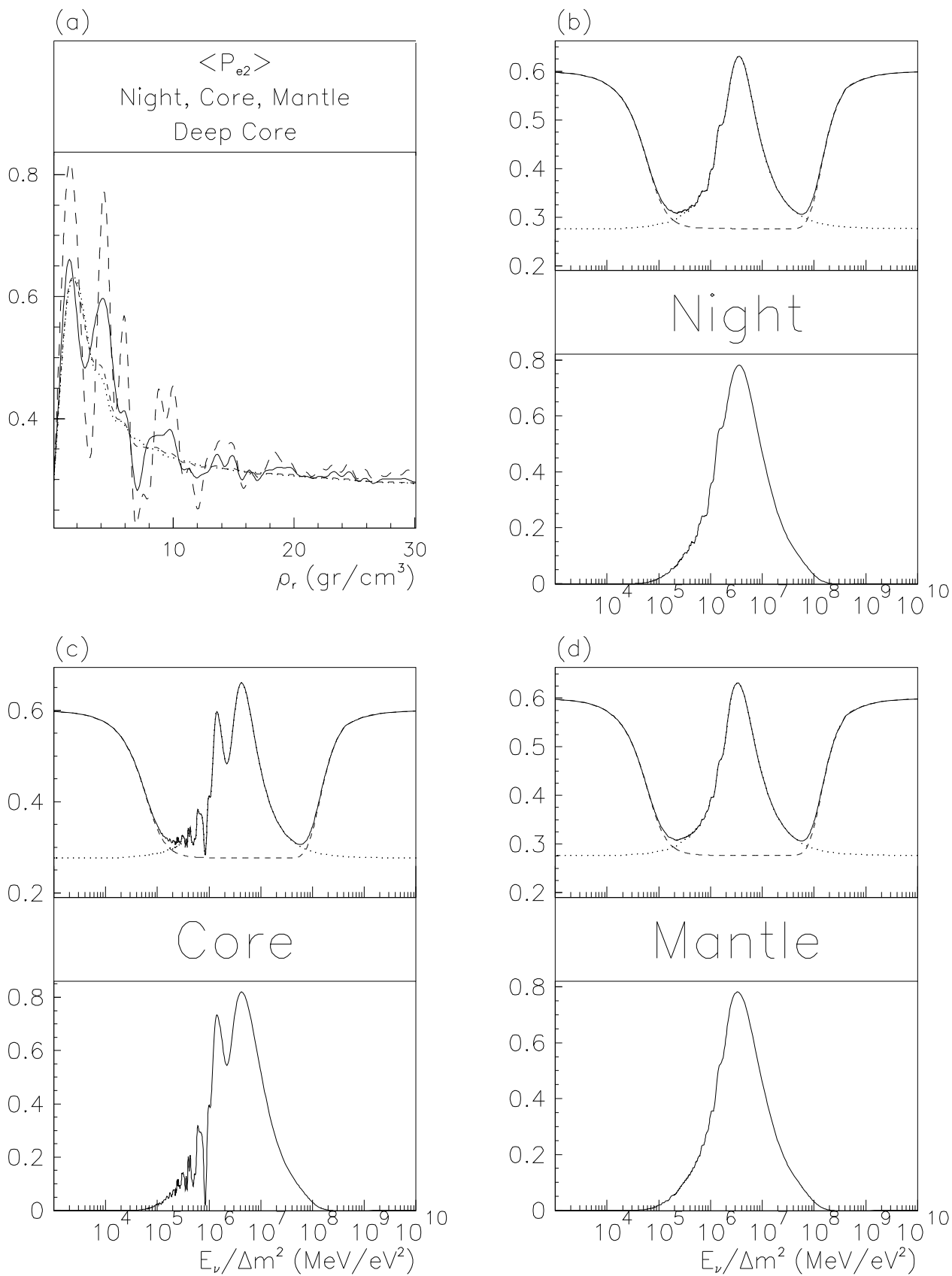


Figure 3.18 $\sin^2(2\theta_\nu) = 0.900$

